THE JOURNAL OF COMPARATIVE NEUROLOGY 226:544-564 (1984)

The Representation of the Visual Field in Parvicellular and Magnocellular Layers of the Lateral Geniculate Nucleus in the Macaque Monkey

MICHAEL CONNOLLY AND DAVID VAN ESSEN
Division of Biology, California Institute of Technology, Pasadena, California 91125

ABSTRACT

Two-dimensional maps of individual layers of the dorsal lateral geniculate nucleus (LGN) in the macaque monkey were constructed and used as a basis for comparing laminar size, shape, and topographic organization. Topographical data from the electrophysiological investigation of the LGN by Malpeli and Baker ('75) were displayed on maps of all six layers. As known from previous studies, there is a significant over-representation of central vision in the LGN. Unexpectedly, though, the visual representation is anisotropic over portions of most LGN layers. That is, the linear magnification factor (millimeters along the laminar surface per degree of visual field) is not equal for all directions from a given point in the visual field. Moreover, the visual representations in the parvicellular and magnocellular divisions of the LGN differ both in their emphasis on central vision and in their anisotropies.

To determine the degree of individual variability, laminar maps were prepared from the LGN of seven other hemispheres. The shapes of laminar maps varied considerably between LGNs, from nearly circular to highly elliptical, but the surface area was relatively constant for each layer. Topographical organization, determined by mapping the optic disc representation on the LGN laminae and by labeling from anterograde and retrograde tracer injections in striate cortex, showed significant individual variability.

Interestingly, the visual representations in the LGN and striate cortex are topologically inverted with respect to one another. This indicates that the establishment of geniculocortical connections involves a systematic crossing-over of fibers.

Information on cell densities and magnification factors in striate cortex obtained from other studies was compared to the results of the present study in order to estimate ratios of cortical neurons to LGN neurons at different eccentricities. The total number of cortical neurons per LGN neuron is about 130 on average, but it extends over approximately a tenfold range, from less than 100 in the far periphery to nearly 1,000 in the fovea. The estimated number of cells in layers 4A and 4Cβ per parvicellular layer neuron is smaller and extends over a slightly narrower range, from 30 to 240, whereas the number of layer 4Cα neurons per magnocellular neuron varies more widely, from about 45 to 7,000.

Key words: primate LGN, topographic organization, laminar organization

The mammalian dorsal lateral geniculate nucleus (LGN) serves as a relay to visual cortex and appears to do relatively little processing of information at the cellular level. Nonetheless, studies of its functional organization have

Accepted January 31, 1984.

Michael Connolly's present address is U.C. San Francisco School of Medicine, S-245, San Francisco, CA.

Address reprint requests to D. Van Essen, Division of Biology, California Institute of Technology, Pasadena, CA 91125.

revealed that visual inputs are rearranged within the LGN in a way that facilitates the subsequent stages of analysis that take place at the cortical level. In the macaque monkey, the LGN has six coaxially arranged layers, each of which receives inputs from one or the other eye. The four dorsally situated parvicellular layers receive inputs from a morphologically and physiologically distinctive group of retinal ganglion cells called "X," or "X-like" cells (Lund et al., '76; Dreher et al., '76; Leventhal et al., '81; Kaplan and Shapley, '82). The upper pair of parvicellular layers contain mainly on-center cells and the lower pair mainly off-center cells (Schiller and Malpeli, '78). Ventrally, there are two magnocellular layers, which receive inputs from "Y", or "Y-like" retinal ganglion cells (Dreher et al., '76) and from a group referred to as X cells but differing functionally from those that project to parvicellular layers (Kaplan and Shapley, '82). The parvicellular and magnocellular divisions of the LGN have different target layers in primary visual cortex (Hubel and Wiesel, '72). Each LGN layer has a topographically organized representation of part or all of the contralateral visual hemifield, and each representation is in precise register with those in neighboring layers (Kaas et al., '72, '78).

While the basic visual topography of the macaque LGN has long been known (see Polyak, '57), there have been no detailed comparisons of the representation in different layers. Malpeli and Baker ('75) made a precise map of visual topography over the entire LGN, but they did not analyze their data in relation to the organization of individual layers. This is largely attributable to the difficulty of dealing with information contained in a large number of histological sections. To alleviate this problem, we have applied to the LGN a technique for constructing accurate two-dimensional representations that was originally developed for cerebral cortex (Van Essen and Maunsell, '80). This has permitted the construction of planar maps of the individual layers of the LGN with little distortion of surface area or linear relationships.

By applying this approach to the data obtained by Malpeli and Baker ('75), we determined the topographic organization of each of the six LGN layers. The results demonstrate significant differences in the visual representation in parvicellular and magnocellular divisions of the LGN. In addition, they provide for interesting comparisons of LGN topography with that of striate cortex, as assessed in a recent study (Van Essen et al., '84), and of the retinal ganglion cell layer, as determined from earlier studies (Van Buren, '63; Rolls and Cowey, '70).

METHODS

The technique for constructing two-dimensional maps of LGN layers is essentially the same as that described elsewhere for representing various regions of cortex (Van Essen and Maunsell, '80). For each LGN, a series of sections, usually at 0.25-mm intervals, was photographically en-

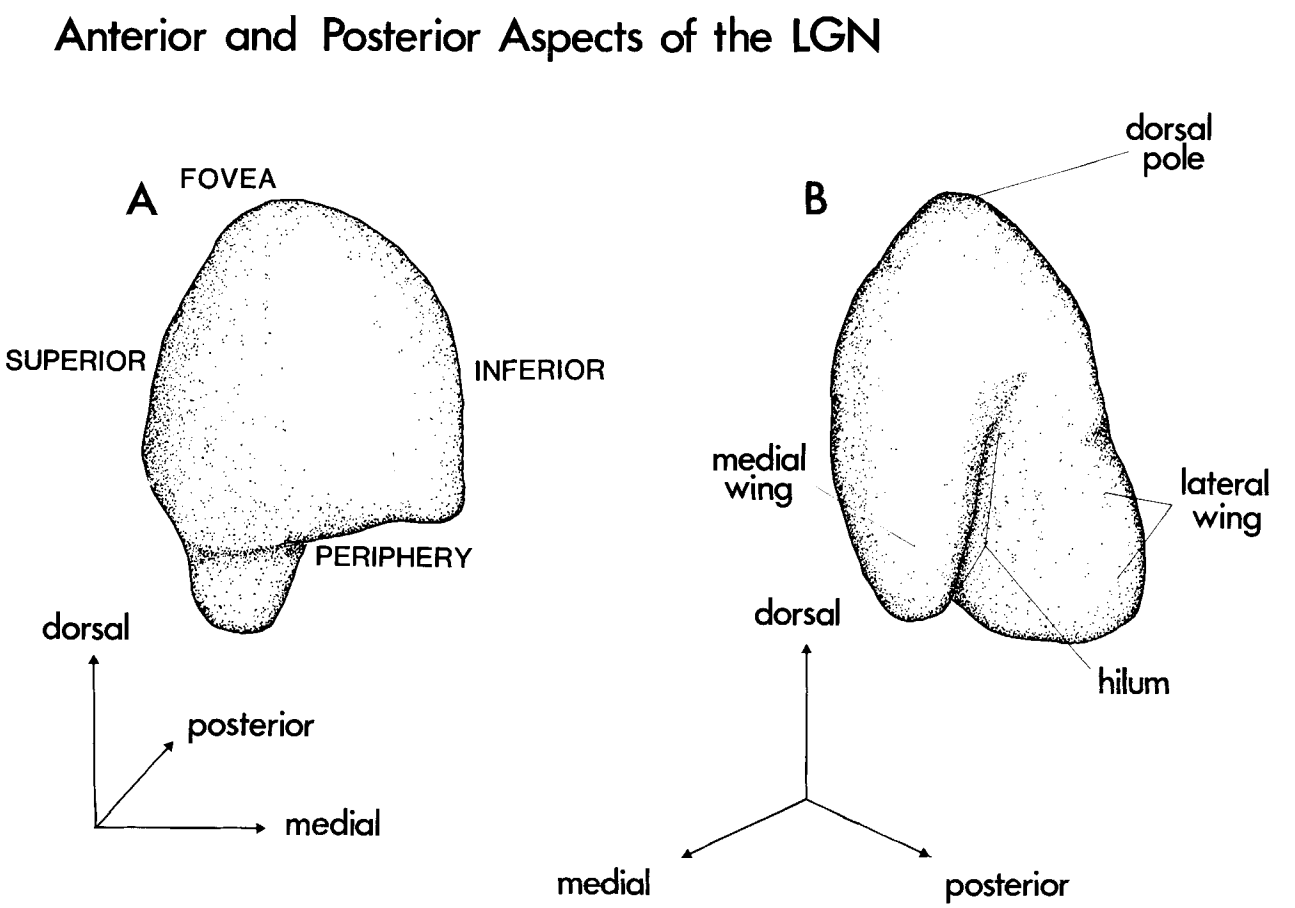

Fig. 1. Anterior (A) and posterior (B) views of a three-dimensional model of a right lateral geniculate nucleus (LGN). The model was constructed from styrofoam pieces cut to match a series of enlarged (×20) horizontal sections of the LGN. The drawings were prepared from photographs of this model. Basic features of topography are portrayed in the anterior view of the LGN: The fovea is represented dorsally, the far periphery ventrally, superior fields laterally, and inferior fields medially. The hilum can be seen as a groove running along the posterior margin of the LGN.

larged (×20, including correction for shrinkage during tissue preparation). Contour lines were drawn through the center of each layer on the enlargements. A separate map for each layer was then constructed by transferring contours onto tracing paper. The length of each contour was preserved, but its shape was changed as necessary to achieve proper spacing between neighboring contours. The resultant laminar maps had minimal distortions of surface area and of the linear relationships between points within a given layer (Van Essen and Maunsell, '80).

Laminar maps were prepared from the LGN of eight hemispheres in seven monkeys. Seven of these cases were from animals used previously for electrophysiological or anatomical investigation of visual cortex in this laboratory, and sections were cut in the horizontal or parasagittal plane. In several cases, injections of [^{3}H]-proline or horseradish peroxidase (HRP) had been made in striate cortex, using techniques described elsewhere (Van Essen et al., '81). The distribution of transported label was plotted on the appropriate laminar maps in order to compare topographic organization in the two structures.

For the one remaining case, the maps were constructed from a particular LGN that had been physiologically mapped in great detail by Malpeli and Baker ('75). Malpeli and Baker obtained their data from a series of vertical penetrations through the LGN. They then plotted isoelevation and isoazimuth curves onto outlines of a series of coronal sections (the plane in which the LGN was cut) and also onto outlines of the LGN in the parasagittal and horizontal Horsley-Clarke planes (their Fig. 5A-C).

The first step in our analysis was to determine the contours of the various layers on the stereotaxic section outlines. In their Figure 3, Malpeli and Baker showed laminar outlines as they appeared before compensation for the shrinkage that occurred during histological processing, and they also showed the overall LGN outlines after shrinkage compensation (i.e., in alignment with stereotaxic coordinates). Using this information, we drew contours through the middle of each layer and then scaled these laminar contours to correct for the 26% linear shrinkage estimated from their drawings. As noted by Malpeli and Baker, it was also necessary to make slight changes in the shape of some contours to correct for a small amount of differential shrinkage within individual sections. The corrected laminar contours were then transferred to the coronal Horsley-Clarke series of their Figure 5A.

At this point, it would have been possible to construct laminar maps directly from the coronal section contours. However, at the time our only experience in making LGN maps was from horizontal sections, and we therefore decided to transfer each set of laminar contours onto the horizontal Horsley-Clarke series illustrated in Figure 5C of Malpeli and Baker ('75). This was done by marking on each laminar contour in the coronal series all points that were also contained in the horizontal series. The points representing a given layer were transferred to the horizontal series and connected to form a set of laminar contours in the horizontal plane. Although this involved an extra stage in the analysis, it was an accurate and complete transformation that did not introduce errors of any significance.

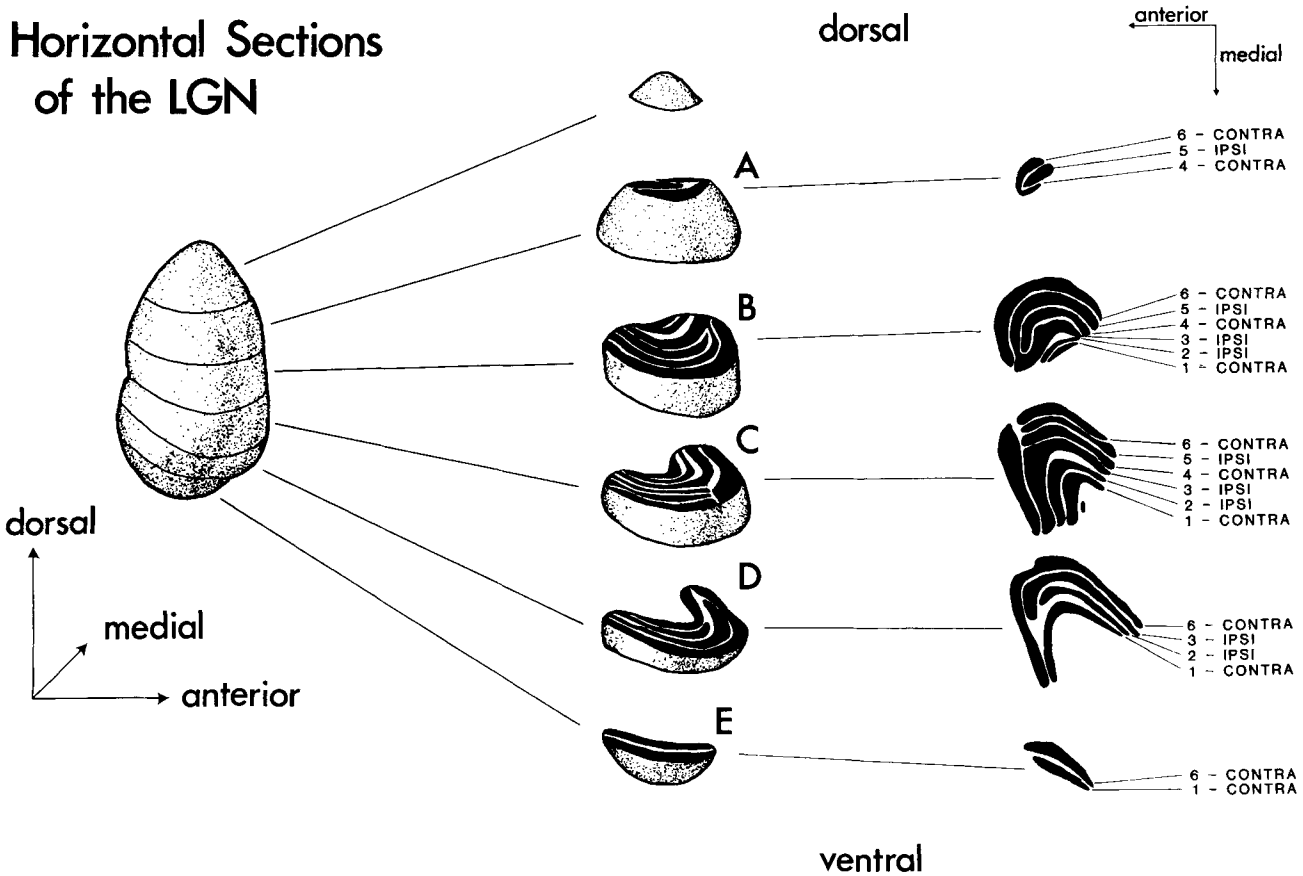

Fig. 2. On the left, an anterolateral view of the model of the LGN. In the center, an exploded view of this LGN, shown at five levels of horizontal section, A through E, taken at intervals of about 1.5 mm. The layers of the LGN are shown here in black. On the right, the same sections have been rotated roughly 180°, and are shown in the plane of the figure, so that medial is down and anterior is to the left in the figure. The contralateral (CONTRA) or ipsilateral (IPSI) eye input and the layer number of each of the six geniculate layers are indicated in the right-most figure.

The three sets of data on visual topography for the different stereotaxic planes are all equally accurate and are equivalent to one another in information content. Indeed, Malpeli and Baker specifically noted that their determination of azimuthal and elevational contours necessitated working simultaneously with data represented in all three planes. Thus, we expect that our results would have been essentially identical no matter which reference plane had been chosen.

RESULTS

Three-dimensional relationships in the LGN

An appreciation of the three-dimensional structure of the LGN is useful for understanding the way in which two-dimensional maps of its layers were prepared. We therefore constructed a scale model of a complete LGN from the right hemisphere, much as was done by Clark ('41). Sketches of this model, made from photographs of anterior and posterior perspectives, are shown in Figure 1. The LGN is roughly half-cylindrical, its long axis running through a groove, the hilum, on its posterior side. In this particular LGN, the long axis runs approximately dorsoventrally, with its upper (dorsal) pole posterior and lateral to the lower (ventral) pole. Malpeli and Baker ('75) reported that there is significant individual variability in LGN orientation, but that in most cases the long axis is tilted considerably more posteriorly than in the example shown here.

The layers of the LGN are themselves roughly half-cylindrical and are coaxial about the hilum. The overall dimensions of the LGN are about 7–9 mm in length (dorsal to ventral), and 9–10 mm in width; the lateral wing extends a few millimeters more ventrally than does the medial wing, so that the overall shape of the LGN is slightly asymmetrical (Fig. 1B).

Basic features of visual topography are indicated alongside the LGN model in Figure 1A. The fovea is represented near the dorsal pole, but slightly to the lateral side, while the far peripheral representation runs along the ventral border of the nucleus. The superior quadrant is represented laterally and the inferior quadrant medially.

The arrangement of layers at different dorsoventral levels of the LGN is shown in Figure 2. On the left is an anterolateral view of the LGN model and in the center, an "exploded" view at five levels of horizontal section. These sections are shown again on the right, rotated so that anterior is to the left and medial is downward; the layers have been numbered and their source of input (contralateral or ipsilateral eye) indicated. Section A, through the dorsalmost tip of the nucleus, grazes only three of the parvicellular layers. All six layers are present in section B and in the lateral part of section C. At level D, which represents a part of the visual periphery, only the four principal layers

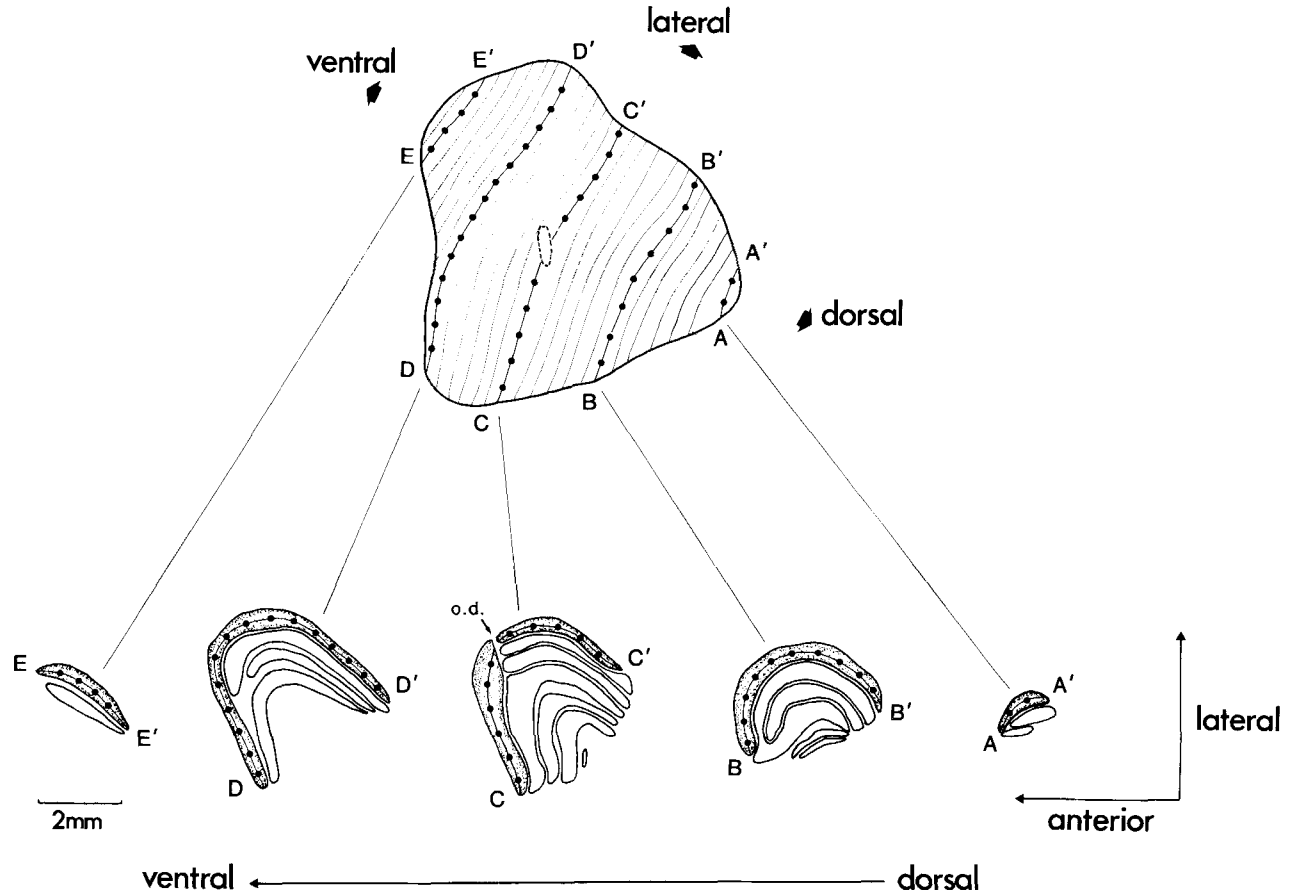

Fig. 3. Above, the two-dimensional map of layer 6, constructed from horizontal sections of the LGN at a spacing of 0.25 mm, and shown in the standard configuration for visual maps, with the foveal representation to the right and the representation of the far periphery to the left. Below, section levels A through E of the model. Dorsal sections are toward the right and ventral sections toward the left. Directions indicated on the map are only approximate, because of the unfolding needed to make a planar representation. The lines with heavy dots show the layer-6 section contours below and their representation on the layer-6 map above. The layer-6 representation of the optic disc can be seen as a gap in section C; its representation on the layer-6 map is shown with a dashed outline.

(6, 3, 2, and 1) are present in the section. This change in layering pattern reflects the fact that layers 4 and 5, the two parvicellular "leaflets," are present only in the region of central visual representation (Kaas et al., '72, '78). The two leaflets are continuous with their respective principal layers (layer 4 with layer 6 and layer 5 with layer 3). The ventral-most section (E) contains only two layers (1 and 6), both of which receive input from the contralateral eye, and thus lies within the representation of the monocular crescent.

Two-dimensional maps of individual layers

A two-dimensional map of layer 6, from the same LGN used to construct the three-dimensional model, is shown in Figure 3, along with the sections labeled A–E from Figure 2. The map has been oriented in the standard configuration adopted in this laboratory for two-dimensional maps (Van Essen and Maunsell, '80): the structure is drawn as though it were from the right hemisphere, regardless of its hemisphere of origin, and as if viewed from the "outside" (from above the pial surface in the case of cortex, and from outside the convex surface in the case of the LGN). The fovea is represented to the right, the periphery to the left, superior fields in the upper half, and inferior fields in the lower half of the map. When the contours of layer 6 are properly aligned, they are nearly straight and parallel to one another. This is because the horizontal sections from which the map is constructed intersect the layer-6 surface at an angle not far from perpendicular.

The relationship between the intact LGN and the two-dimensional representations of its layers is illustrated in Figure 4. The sequence begins with an anterior view of the LGN model (Fig. 4A). In Figure 4B, layer 6 alone is seen from the same perspective. The contours correspond to section levels A–E of Figures 2 and 3. The process of preparing a two-dimensional representation of a layer is conceptually similar to "unfolding" its half-cylindrical shape to lie in one plane (arrows, Fig. 4B). The actual two-dimensional map of layer 6, prepared from section contours, is shown in Figure 4C in an orientation equivalent to that which would be obtained from a completed unfolding of Figure 4B. It is shown again in Figure 4D, where it has been rotated 90° clockwise to conform to our standard format for visual maps.

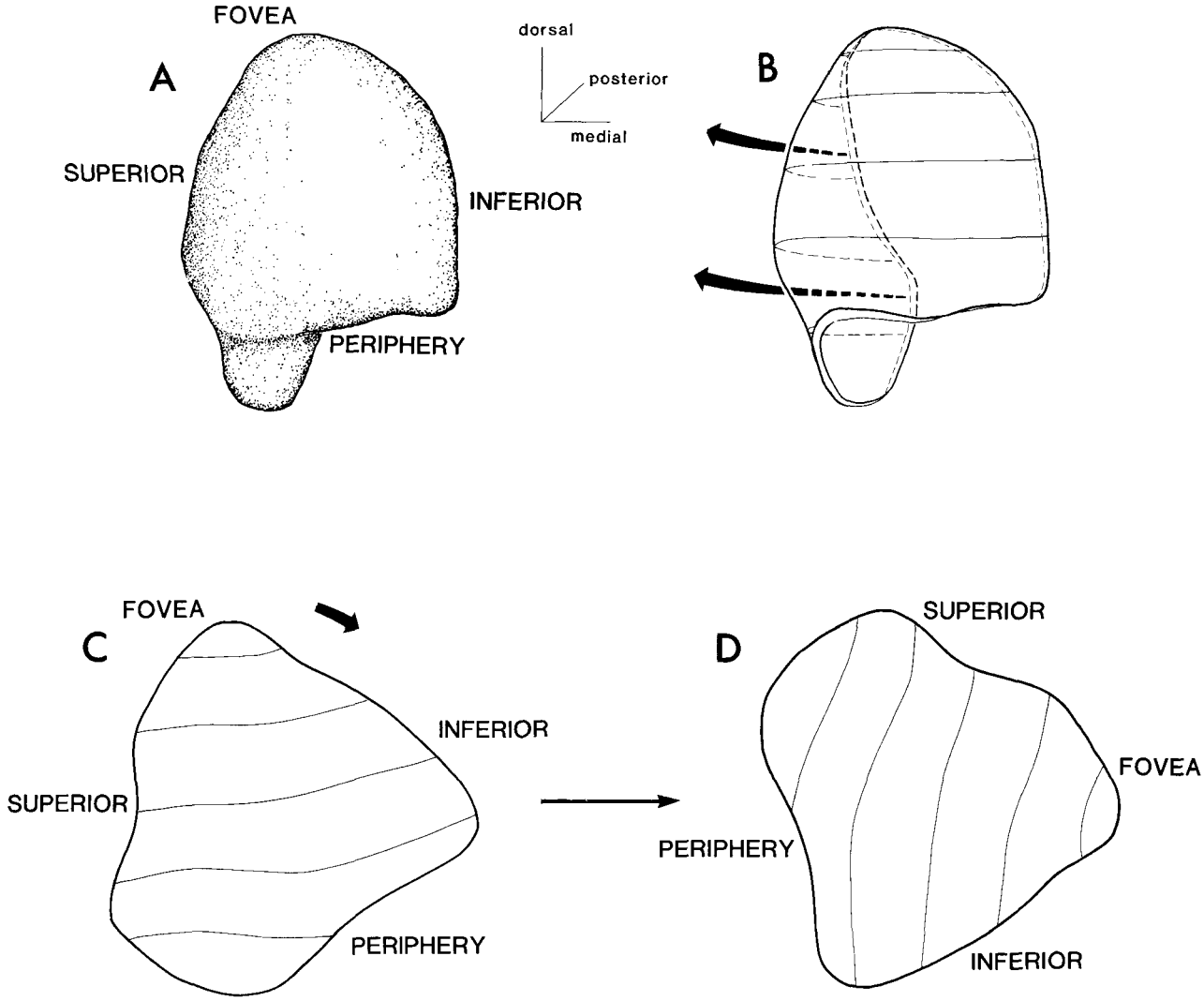

Fig. 4. The relationship between layer 6 of the intact LGN and its two-dimensional laminar map. A. An anterior perspective of the LGN model. B. Layer 6 alone is shown. The arrows show the lateral wing of layer 6 being "pulled" into one plane with the medial wing. C. The two-dimensional map of layer 6, oriented to correspond to the unfolded layer 6 of B. D. The map has been rotated roughly 90° to lie in the standard configuration, with the foveal representation on the right. Superior fields are represented on the upper half of the map, inferior fields on the lower.

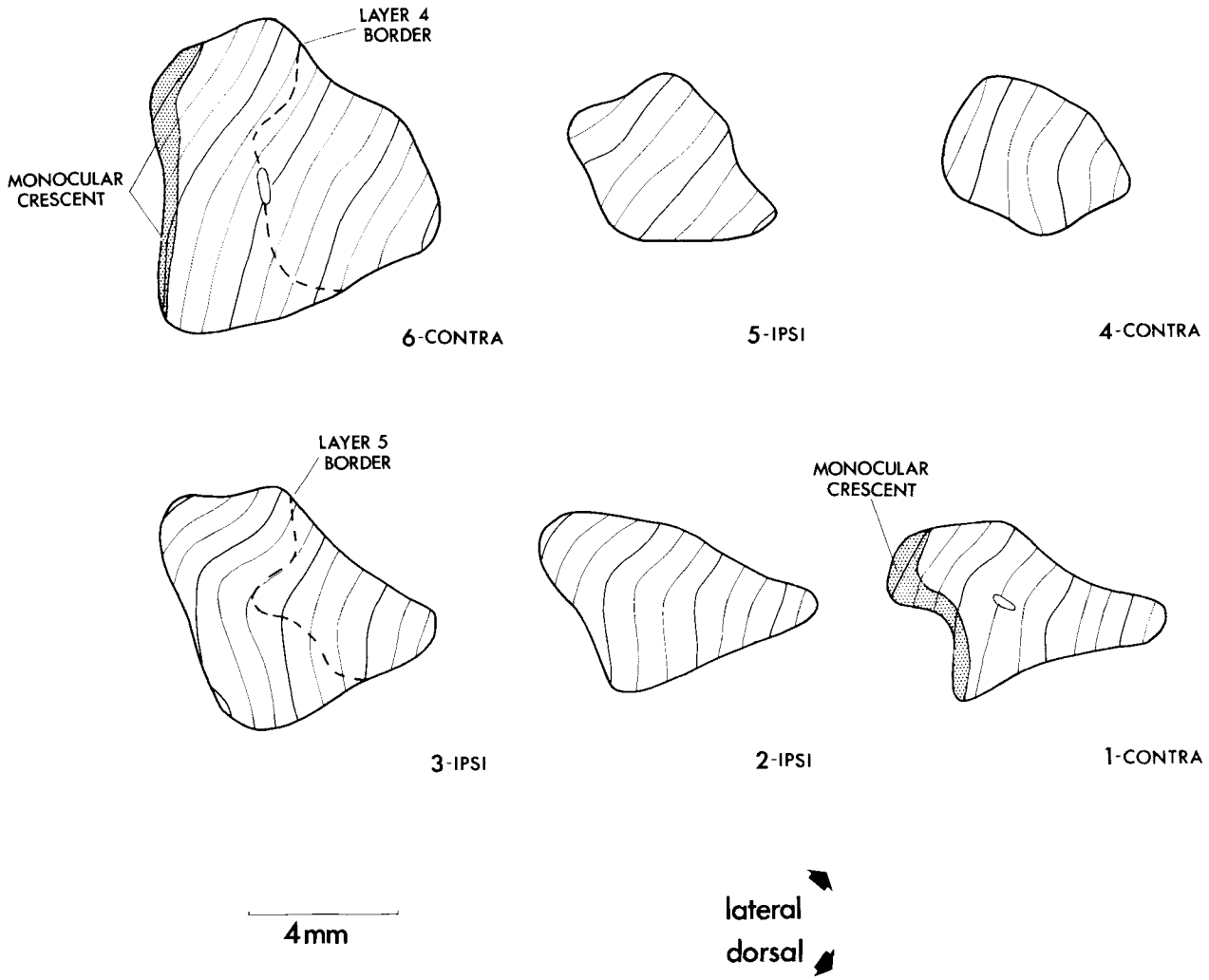

Fig. 5. Maps of all six magnocellular and parvicellular layers of the LGN. The number and eye input (ipsilateral or contralateral) for each layer are indicated below it. The illustrated contours on the laminar maps are from horizontal sections taken at intervals of 0.5 mm. The representation of the optic disc is shown on the maps of layers 1 and 6 by fine stippling. The monocular crescent region is indicated by coarse stippling on the same two layers. The broken lines on the layer 3 and layer 6 maps show the lines of fusion between these layers and their leaflets, layers 4 and 5, respectively.

When a hemispherical surface such as the retina is physically flattened into a two-dimensional sheet, cuts or tears are introduced to alleviate shear (linear distortions). Fortunately, it was possible to make accurate two-dimensional representations of LGN layers without any such discontinuities. The explanation for this lies in fact that the individual layers are more like half-cylinders than hemispheres, as was illustrated in Figure 4B. Thus, they have little intrinsic curvature and can be unfolded with only modest distortion, the magnitude of which is discussed in the following section.

Figure 5 shows two-dimensional maps of all six layers from the same LGN. As expected, the layers differ markedly in surface area. Layers 6 and 3, the two parvicellular principal layers, are largest. The parvicellular leaflets, layers 4 and 5, are somewhat smaller, extending only over the representation of central fields in the LGN. The magnocellular layers are smallest because of their inner position in the coaxial arrangement of layers.

The monocular crescent representation is indicated by stippling for layers 1 and 6; it forms a narrow strip along the ventral edge of each layer. Also shown, as outlined regions on these two maps, are the small cell-free zones corresponding to the optic disc on the retina. For both layers, this discontinuity is located midway mediolaterally and slightly closer to the ventral than to the dorsal pole. Interestingly, the layer-6 discontinuity is located very close to the lines of fusion between the leaflets and their principal layers, which are shown as dashed lines on the maps of layers 3 and 6.

Maps of visual topography

In order to study the detailed topographic organization of individual LGN layers, we constructed maps of all six layers using the results of an electrophysiological investigation of the LGN by Malpeli and Baker ('75). The usefulness of planar maps for analysis of visual topography depends crucially, of course, on the accuracy with which they reflect spatial relationships in the intact LGN. We therefore attempted on each map to minimize any distortions of areal and linear relationships. Figure 6A shows a map of layer 6 prepared from Malpeli and Baker's ('75) data, as described in "Methods." Using an approach outlined in the legend to Figure 6 and described in more detail elsewhere (Van Essen

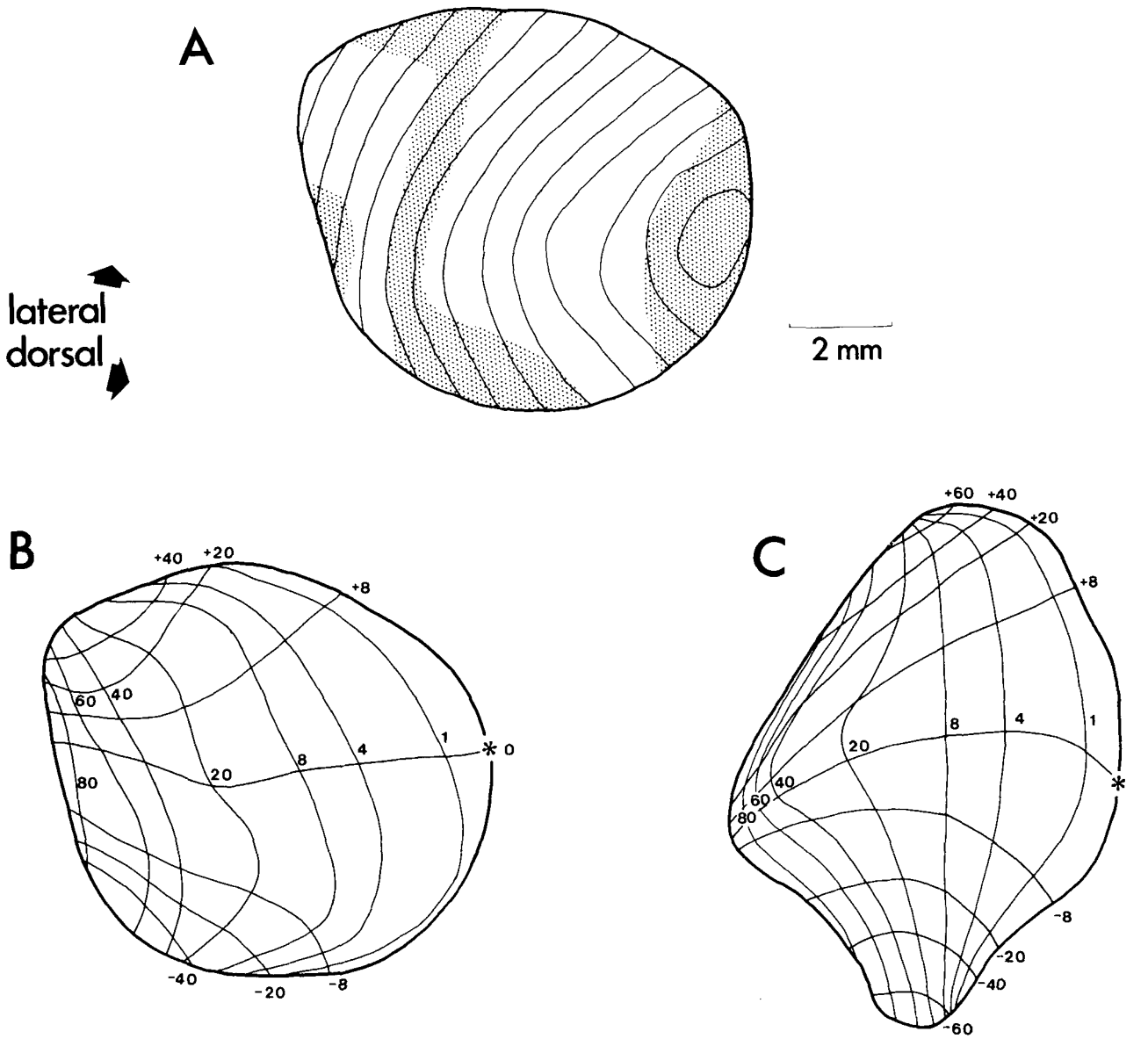

Fig. 6. A. The map of layer 6 prepared from Malpeli and Baker's ('75) horizontal Horsley-Clarke series through the LGN (their Fig. 5c). Horizontal sections were used instead of the coronal sections in which the LGN had originally been cut because of the greater ease with which two-dimensional maps could be made (see "Methods"). The outlines of layer 6 were determined by translating from the coronal sections shown in their Figure 3, using the Horsley-Clarke coordinates provided in both coronal and horizontal planes as a basis for the transformation. Linear distortions in 20 places on the map were estimated by comparing the distances between pairs of points on neighboring contours of the map with the actual distances in the intact LGN, as determined from the stereotaxic coordinates of these points (cf. appendix to Van Essen and Maunsell, '80). Regions where linear distortion exceeds 10%, indicated by stippling, occupy 30% of the map. Only 10% of the map is associated with a distortion of more than 20%. Areal distortions were calculated in a similar fashion by comparing actual laminar areas with corresponding map areas. Areal distortions are nowhere larger than 10% on this map. B. The two-dimensional map of layer 6. Each representation is overlayed with isoazimuth and isoelevation contours. C. Malpeli and Baker's ('75) "semi-schematic" representation of the dorsal surface of the LGN (their Fig. 8), most of which is layer 6. The map is based on a modification of their orthographic projection of the dorsal surface (their Fig. 7); its orientation has been reversed to conform to the format used in the present study.

and Maunsell, '80, appendix), we calculated the magnitude of both areal and linear distortions at many points over the whole map. This analysis indicated that the representation of surface area is accurate to within ±10% of actual laminar area over the entire map. Over most of the map linear distortions are also less than 10%, but in a few regions, noted by stippling in Figure 6A, there are linear distortions of 10–30%.

Malpeli and Baker ('75) illustrated the results of their electrophysiological mapping by marking isoazimuth and isoelevation contours on a series of sections through the LGN. We transferred these topographic contours onto the map of layer 6, as shown in Figure 6B. For comparison, Figure 6C shows Malpeli and Baker's ('75) planar representation, which is based on a schematic flattening of the dorsal surface of the LGN. The two versions are similar in their representation of central vision, but they deviate significantly from one another in the representation of the periphery. Much of this discrepancy can be attributed to distortions along the margins of Malpeli and Baker's ('75)

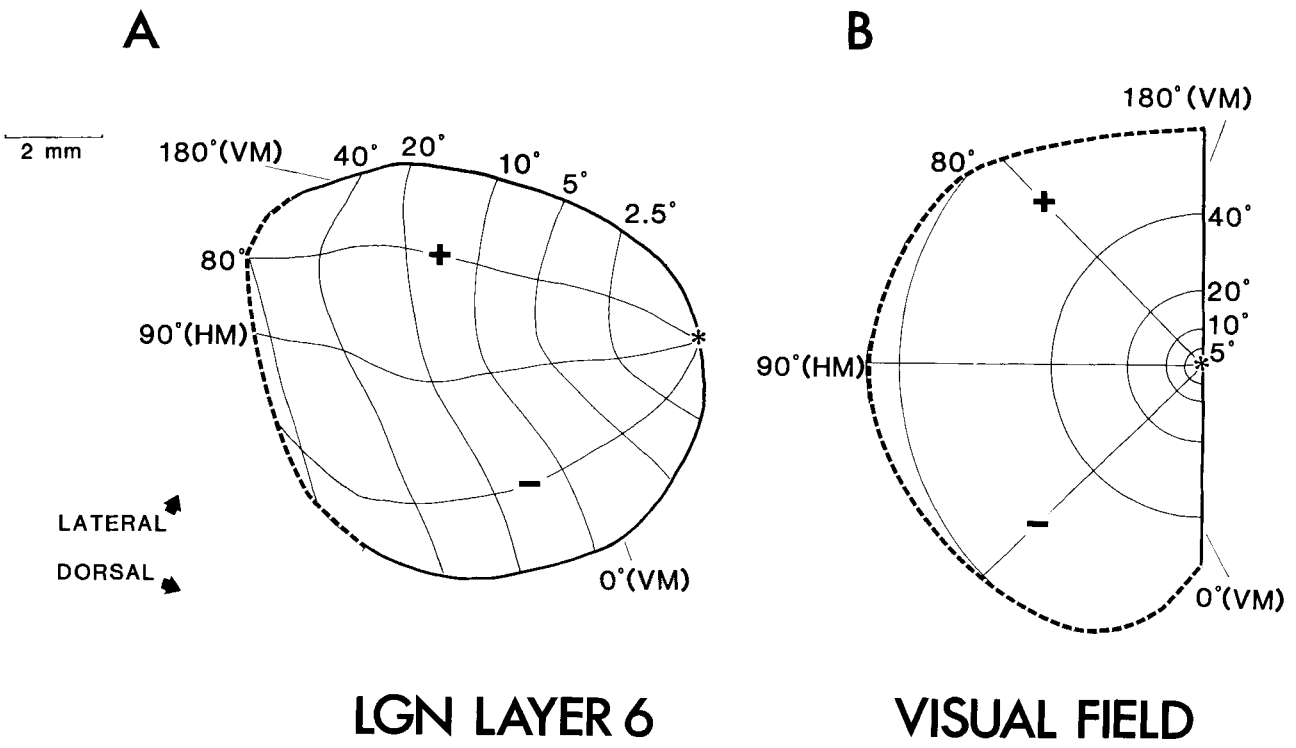

Fig. 7. At left, the two-dimensional map of layer 6 prepared from Malpeli and Baker's ('75) data; at right, for comparison, the visual field of the macaque, measured by Malpeli and Baker ('75), and represented in two dimensions. Both are shown in spherical coordinates with lines of isoeccentricity, from 2.5° to 80°, and lines of isopolar angle, from 0° (the inferior vertical meridian) to 180° (the superior vertical meridian), at 45° intervals. The fovea and its layer-6 representation are marked by the asterisks. HM, horizontal meridian (90° polar angle). The far periphery of the visual field and its layer-6 representation are shown by dotted lines.

map (see legend to their Fig. 8). To best assess LGN topography, particularly that of central vision, we transformed the azimuth and elevation coordinates from Malpeli and Baker's ('75) LGN sections to spherical polar coordinates. Figure 7A shows the layer-6 map with its visual representation denoted by lines of constant eccentricity and constant polar angle; for comparison, Figure 7B shows a representation of the contralateral visual hemifield in the same coordinate system. Because of the overemphasis on central vision, the inferior and superior vertical meridians (0° and 180° polar angle, respectively) occupy more than 80% of the map's perimeter; the corresponding figure for the visual field is only 30%. The horizontal meridian representation (90° polar angle) divides the map of layer 6 into two nearly equal parts, with slightly more area devoted to the inferior than to the superior quadrant (53% vs 47%). Lines of constant eccentricity and constant polar angle intersect each other nearly orthogonally on the LGN map, as they do in the visual field itself. Lines of isoeccentricity are approximately parallel to one another and of comparable length for eccentricities greater than 5–10°.

In Figure 7B, the visual hemifield is divided into four sectors by the horizontal meridian and the 45° and 135° isopolar contours. Inside 60° eccentricity, these four sectors are equal in area in the visual field, but their representations in layer 6 are markedly unequal. The two sectors adjoining the horizontal meridian (45–90° and 90–135° polar angle) are largest (31 and 26%, respectively, of total laminar surface area), whereas the sectors adjoining the vertical meridian (0–45° and 135–180° polar angle) each occupy only 21% of total map area. Thus, the visual representation in the LGN deviates significantly from radial symmetry.

Maps of all six layers prepared from Malpeli and Baker's sections ('75) are illustrated in Figure 8. In order to discern local features of topography, the visual field was divided by a "spiderweb" pattern of isoeccentricity and isopolar lines into small, approximately square compartments whose areas increase as the square of eccentricity (Fig. 8A). Figure 8B shows how this grid is mapped onto each LGN layer. Numerous similarities among all the maps are evident, but there are also some important differences. The representation of central vision is significantly greater for the parvicellular than for the magnocellular layers, as has been indicated by stippling the central 5° representation on each laminar map in Figure 8. As expected from earlier studies (Kaas et al., '72, '78), the leaflets represent eccentricities only out to 15–25°.

The overemphasis on fields near the horizontal meridian, already noted for layer 6, is noticeable in all four parvicellular laminae, but not in the two magnocellular laminae. Similarly, the small overemphasis in representation of the inferior quadrant of the visual field is shared by the parvicellular but not by the magnocellular layers. The layers of the LGN that are innervated by the contralateral eye (layers 1, 4 and 6) have a larger total surface area than do the ipsilaterally innervated layers (layers 2, 3 and 5), about 60% of total LGN map area. This bias is particularly noticeable in the region of peripheral representation (beyond 20° eccentricity), where total contralateral map area is nearly twice as large as total ipsilateral area.

Anisotropies in the representation of the visual field. Although the compartments of the visual field in Figure 8 are all identical in shape, their representations in the LGN vary considerably, from nearly square to highly elongated along one axis or the other. In regions where the

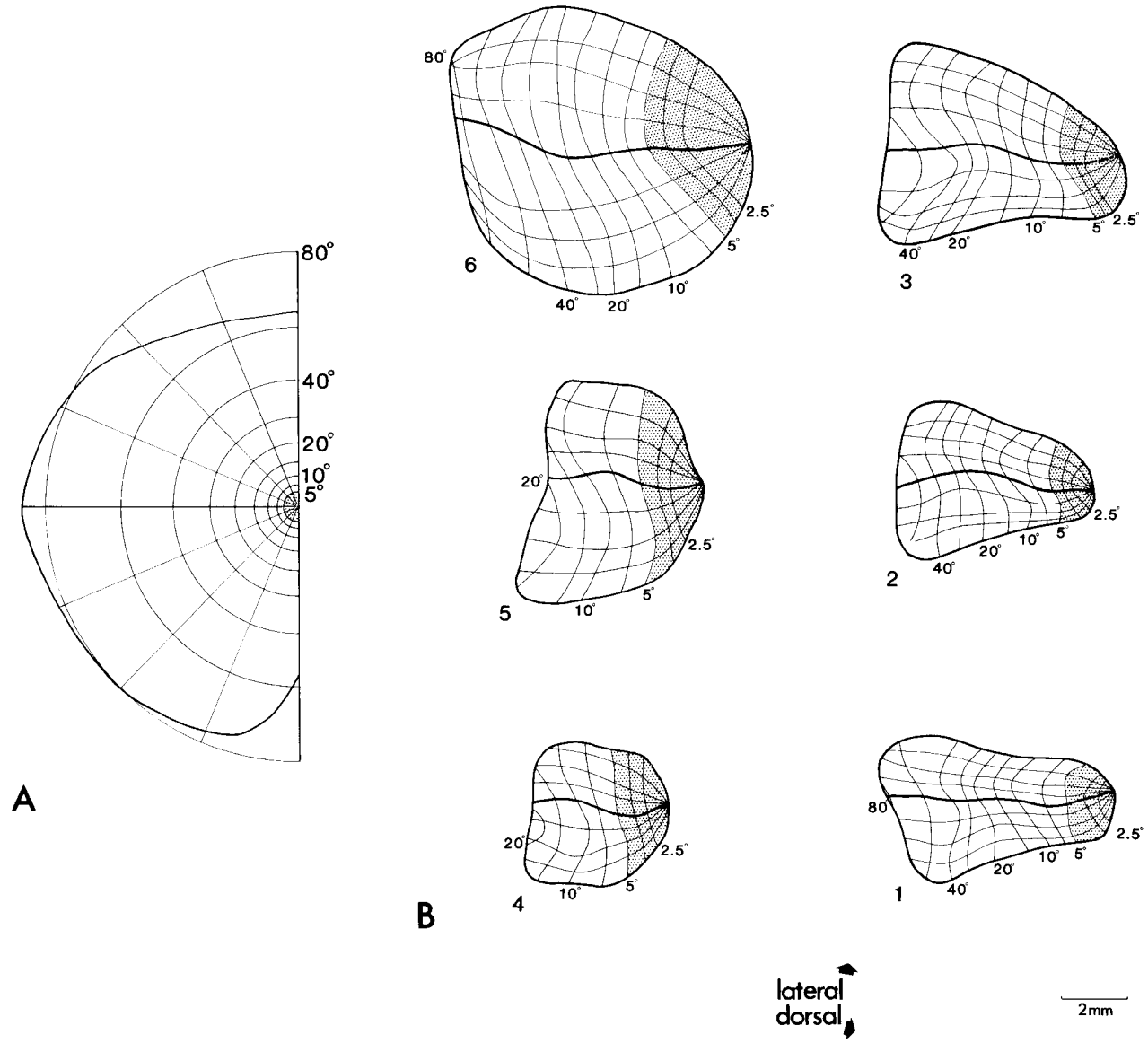

Fig. 8. A. The visual field divided by a grid of isoeccentricity and isopolar angle lines into regions that are approximately square. The perimeter of the visual field (Malpeli and Baker, '75) is shown as a darkened line. The central 5° of the visual field has been stippled. B. The same gridwork of lines is shown overlain on maps of the six layers of the LGN. Maps of each layer were prepared in the manner described in the legend to Figure 6. The region of each layer that represents the central 5° of the visual field has been stippled.

compartments are square, the linear magnification factor (millimeters of map length per degree of visual field) is independent of the direction along which it is measured, and the visual representation is therefore locally isotropic. This is approximately the case along the vertical meridian representation in layer 6 and along parts of the horizontal meridian representation in layers 1 to 3. In other regions, the compartments are distinctly elongated; there, the visual representation is anisotropic and the magnification factor is greatest along a compartment's long axis and least along its short axis. In layer 6, anisotropies are largest along the peripheral horizontal meridian representation, where the magnification is two to three times greater along isoeccentricity contours than along isopolar contours. In the more ventral layers, the anisotropies are most pronounced along the vertical meridian, and the magnification factor is greater along isopolar contours than along isoeccentricity contours. This pattern is related to the cylindrical geometry of the LGN, as will be considered further in "Discussion." Overall, these results indicate that anisotropies of the visual representation in the LGN are substantial in some regions, and that they depend on layer, eccentricity, and polar angle.

Accuracy of the maps. At this stage it is appropriate to comment on the overall accuracy that can be ascribed to the results illustrated in Figure 8. Malpeli and Baker's study is a notably careful and thorough analysis of topographic organization in a visual structure. Nonetheless,

their analysis involved extensive interpolation between data points for different recording sites, using the assumption that linear interpolations over short distances were valid, and it also involved smoothing of tiny irregularities in the mapping. Superimposed on this are whatever additional errors that were contributed by our procedure for constructing laminar maps. These include minor uncertainties in identifying layers in regions where the LGN was cut tangentially and in compensating correctly for the small degree of differential shrinkage of sections (see "Methods"). In addition, it was noted above that the construction of the planar maps involved distortions of up to 10%, in the representation of surface area as well as distortions of up to 30%, but usually less than 10% in representing linear relationships. Finally, there might have been small errors in transposing to polar coordinates from the azimuth/elevation coordinates used by Malpeli and Baker.

Ideally, one would like to summarize this analysis of errors by generating uncertainty limits for the topographic contours and the map outlines for each layer. Unfortunately, this is not feasible, given the difficulty of judging the magnitude of some sources of error. There are sure to be some regions of the maps in which local irregularities have been artifactually introduced and other regions in which genuine irregularities have been inadvertently smoothed. Nonetheless, we are confident that there are no large errors that have been overlooked and that the concatenation of the various small and unavoidable errors has not led to severe distortions in the maps that would seriously affect our major conclusions.

Cellular magnification factors in the LGN

Our primary goal in the present study was to obtain an accurate description of the visual representation in individual LGN layers. In studies of cortical sensory areas, the standard approach has been to calculate the magnification factor as either a linear measure (millimeters cortex/degree visual field) or an areal measure (mm^2/deg^2 visual field). The utility of these measures is dependent on the fact that cortical thickness and cell density are relatively constant within any given sensory area. Hence, the areal magnification factor generally is proportional to the number of cells available for processing inputs from a particular part of the visual field. In the LGN, however, the situation is complicated by the fact that cell density and laminar thickness vary across, and sometimes within, layers. It was therefore necessary to take these parameters into account when determining the cellular representation for different parts of the visual field.

To approach this problem we first calculated mathematical expressions for areal magnification factors as a function of eccentricity in each LGN layer, using a procedure similar to that applied to striate cortex in an earlier study (Van Essen et al., '84). The areal magnification factor was determined by taking the ratio of the area of a compartment in an LGN layer to the area of the corresponding visual field compartment in Figure 8. For all layers, the size of compartments increases sharply with eccentricity for the central 5° and more slowly at higher eccentricities. Given that the visual field compartments were chosen to increase as the square of eccentricity, it follows that the areal magnification factor (mm^2 LGN/deg^2 visual field), has a dependence on eccentricity that is less steep than an inverse square relationship. For layer 6 this relationship was determined by least squares fitting to a power function to be

$$1)\ M_a = 2.1\ E^{-1.7}\ mm^2/deg^2 \qquad \text{(layer 6; } E > 2.5°\text{)}$$

where M_a is the areal magnification and E is eccentricity, with only eccentricities greater than 2.5 included in the analysis. For layer 1 the corresponding expression is

$$2)\ M_a = 0.4\ E^{-1.5} \qquad \text{(layer 1; } E > 2.5°\text{)}.$$

In order to convert expressions of areal magnification to cellular magnification it was necessary to determine laminar thickness and cell density as functions of eccentricity for each layer. Laminar thickness was measured in three individual LGNs in regions where the sectioning plane was approximately normal to the laminar surface. The average values after shrinkage correction were 150 μm for layer 1 (range 130–180 μm), 125 μm for layer 2 (range 100–150 μm), 225 μm for binocular portion of layers 4 and 6 (range 200–270 μm), 175 μm for their monocular portions, and 175 μm for the parvicellular leaflets, 3 and 5 (range 140–200 μm). Aside from the difference between monocular and binocular portions of layer 4 and 6, there was no consistent gradient in thickness within individual layers.

In order to assess cell density in different layers, we relied on published data, because the frozen-sectioned material available in our laboratory was not satisfactory for making accurate cell counts. Clark ('41) reported that cell density is constant in the magnocellular layers but varies over a twofold range in the parvicellular layers (due to progressive changes in the degree of invasion by optic tract fibers). His values were not corrected for tissue shrinkage during histological preparation, so we estimated the appropriate correction factor by comparing the total volume of LGN layers calculated by Clark (29 mm^3, excluding interlaminar zones) with that from Malpeli and Baker's ('75) study. Malpeli and Baker reported a total LGN volume of 77 mm^3, and our planimetric measurements on their section drawings indicate that 56 mm^3 (73%) was in the cell layers. Scaling of Clark's cell density measurements by the resultant correction factor of 0.52 yields values of 21,000 cells/mm^3 for the magnocellular layers and 27,000–60,000 for the parvicellular layers.

Once these values were obtained, the appropriate calculations were made to determine the number of LGN cells in each of the compartments shown in Figure 8. Expressions for cellular magnification factor (M_c, cells/deg^2) for eccentricities outside the fovea were derived by least-square fitting to power functions of the form $M_c = kE^{-x}$. Near the foveal representation the magnification factor has a much less steep dependence on eccentricity. To adjust for this, the expressions for magnification were modified in the same way as was done for striate cortex (Van Essen et al., '84), by making $M_c = k(a + E)^{-x}$. The value of the additive constant "a" was chosen to yield the appropriate total number of cells in the central 2.5° (based on the known surface area, thickness, and cell density in this region). Values of k, a, and x for each layer are provided in Table 1. We also derived expressions of cellular magnification as a function of eccentricity for all parvicellular layers combined, for the two magnocellular layers, and for the entire LGN. Table 1 also shows the total number of cells calculated for different

LGN layers. The cell counts for eccentricities greater than 2.5° were obtained by integration of the power function over the appropriate range. For the central 2.5° the cell counts were obtained by calculating the product of surface area, laminar thickness, and average cell density. The total number of LGN neurons (1.3 million) and the numbers of paravicellular neurons (1.2 million) and magnocellular neurons (0.14 million) are all slightly smaller than the 1.6×10^6 estimated by Clark ('41) and slightly larger than the 1.1×10^6 estimated by Chow et al. ('50). The ratio of parvicellular to magnocellular neurons (7.8) is slightly greater than the value of 6.5 determined for *Cercopithecus* by Hassler ('66).

Curves for the parvicellular and magnocellular expressions, along with the data points from which they were derived, are shown in Figure 9. In comparison to the areal magnification factors for individual parvicellular layers (cf. equation 1), the most significant difference for the parvicellular layers as a whole is the steeper dependence on eccentricity. This is due to several factors, including the facts that 1) two of the parvicellular layers (4 and 5) are restricted to the representation of the central 15°, 2) parvicellular cell density is decreased in the periphery, and 3) laminar thickness is decreased in the monocular crescent.

It is important to consider what additional errors may have been introduced in making the transformation from areal magnification to cellular magnification factors and how this affects the accuracy of the data presented in Figure 9 and Table 1. One source of error that has already been discussed is inaccuracy of various sorts in the laminar maps illustrated in Figure 8. Additional sources include inaccuracies in determining laminar thickness and cell density. The estimates of laminar thickness are unlikely to be in error by more than 15–20%, given the range encoun-

TABLE 1.[1]

Layer	k	a	x	No. of cells[2] Outside 2.5°	Inside 2.5°	Total
6	26,800	0.80	1.86	430,000	61,000	490,000
5	6,600	1.96	1.46	200,000	16,000	220,000
4	6,470	1.01	1.50	120,000	16,000	130,000
3	7,380	0.88	1.56	260,000	21,000	280,000
Total parvicellular	83,700	1.28	1.96	1,000,000	110,000	1,100,000
2	1,170	2.25	1.44	60,000	1,700	62,000
1	1,980	3.94	1.54	81,000	1,400	82,000
Total magnocellular	3,520	3.12	1.56	140,000	3,100	140,000
Total LGN	82,400	1.31	1.90	1,200,000	120,000	1,300,000

[1]Parameters k, a, and x refer to the equation used to relate the cellular magnification factor, M_c, to eccentricity, E:

$$M_c = k(a + E)^{-x}.$$

[2]All estimates of cell number were originally calculated to three places and have been rounded off to two significant digits.

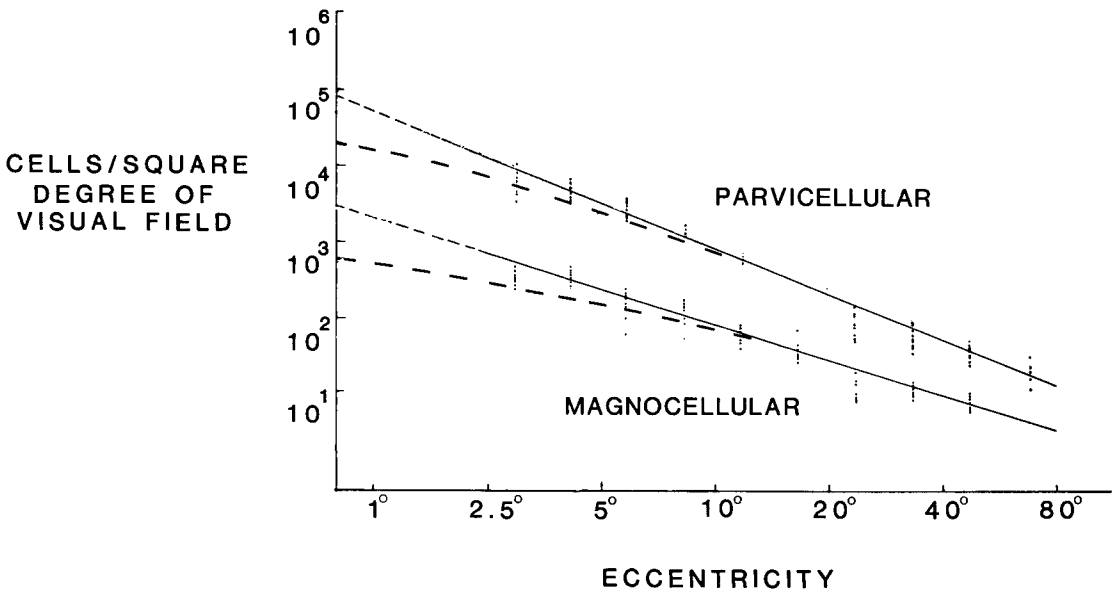

Fig. 9. Total parvicellular and magnocellular representations of the visual field, in number of cells per degree of visual field, as a function of eccentricity. The areas of laminar compartments (Fig. 8) were used along with estimations of cell density and laminar thickness to determine the number of cells per degree of visual field for each compartment (see text), shown as data points here. Lines of best fit were determined for total parvicellular representation (layers 3 through 6) and total magnocellular representation (layers 1 and 2) beyond 2.5° eccentricity. The curved lines show the cellular magnification factors for the foveal region, based on the equation $M_c = 8.37(1.28 + E)^{-1.96} \times 10^4$ for the parvicellular layers and $3.52(3.1 + E)^{-1.56}$ for the magnocellular layers (see text for explanation of derivation).

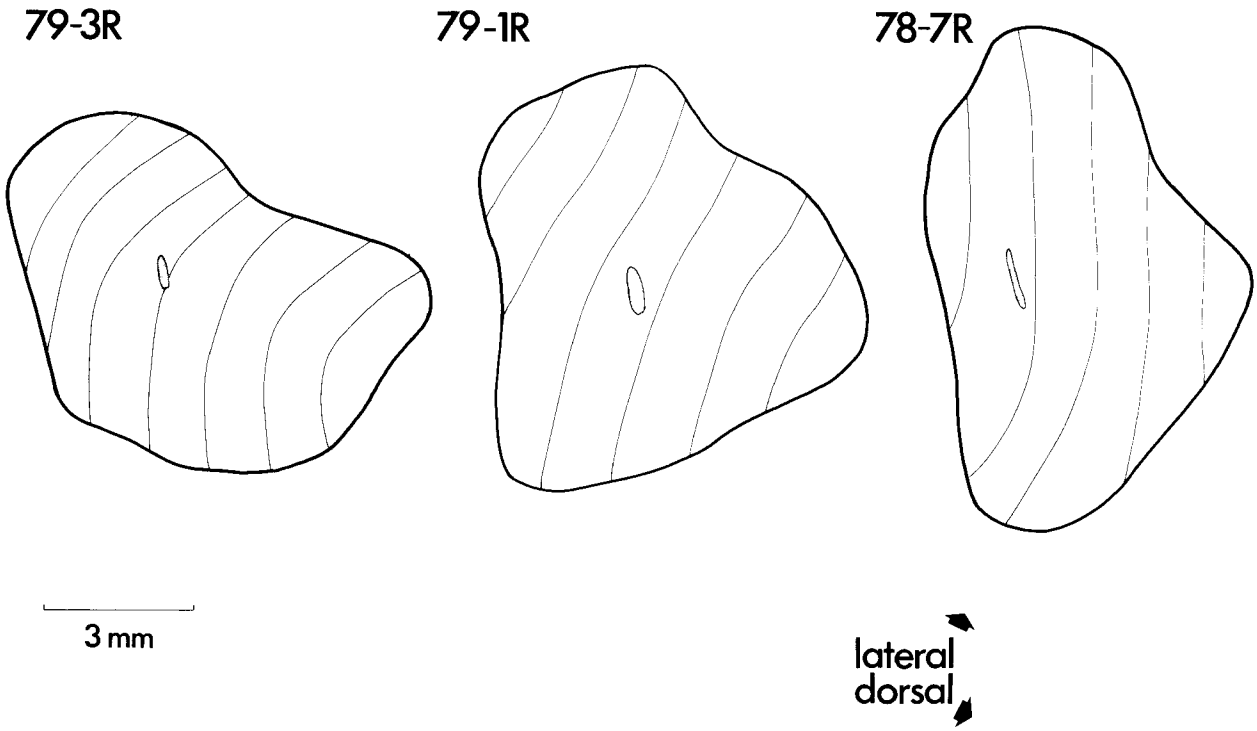

Fig. 10. Two-dimensional maps of layer 6 in three individuals, which demonstrate the variability in shape of the geniculate laminae. Layer 6 of LGN 79-3R is somewhat elongated dorsoventrally, while layer 6 of LGN 78-7R is considerably elongated mediolaterally. The dimensions of layer 6 of LGN 79-1R lie between these extremes. The optic disc representations in each layer have been stippled.

tered in different measurements. For cell density, it is important to draw a distinction between relative and absolute errors. Relative errors, in terms of the variations in cell density within parvicellular and magnocellular laminae, are likely to be less than 20%. Absolute errors might be somewhat larger, given the indirect way in which we estimated the appropriate shrinkage correction factor for Clark's ('41) data. Nonetheless, the fact that our calculated value for the total number of LGN neurons is in reasonable agreement with other published estimates suggests that the absolute errors in our analysis were not unduly large. Taking these various factors into consideration, we estimate that the assorted cell counts shown in Table 1 are accurate to within ±30–50%. Accordingly, the estimates of cell number are shown to only two significant digits.

Individual variability

Previous studies have demonstrated considerable individual variability in the size, shape, and topographic organization of striate cortex and MT in the macaque (Van Essen et al., '81, '83). To assess variability in the LGN, we prepared laminar maps for the LGN in seven other hemispheres, all from animals that had been used previously for anatomical studies in this laboratory. In each LGN, the outermost layer, layer 6, was largest (mean 45 mm^2, range 40–55 mm^2); layer 3 was about two-thirds as large (mean 28 mm^2, range 25–30 mm^2), and each of the magnocellular layer and the parvicellular leaflets were about one-half as large as layer 6 (layer 1: mean 19 mm^2, range 16–22 mm^2; layer 2: mean 21 mm^2, range 18–26 mm^2; layer 4: mean 15 mm^2, range 13–18 mm^2; layer 5: mean 19 mm^2, range 15–25 mm^2). Thus, for a given layer, there is only modest individual variability in surface area (±15-20% of the mean). However, there is considerably more variability in laminar shape, as is demonstrated by the three representative maps of layer 6 in Figure 10. While the areas of layer 6 maps vary by less than 40%, their shapes range from roughly circular to highly elliptical. The ratio of total ipsilateral to contralateral eye laminar area in the LGN varied only slightly: the percent of total laminar area innervated by the contralateral eye ranged from 52 to 60% in the eight cases mapped. The percent of total laminar area which was magnocellular was also relatively constant, ranging from 23 to 30%.

In most cases examined, injections of ^{3}[H]-proline or HRP had been made in striate cortex; these agents were transported to the LGN through geniculocortical or corticogeniculate fibers. Labeled regions were plotted on maps of individual layers. The sites of injection had been plotted on maps of striate cortex, the topographic organization of which is known (Daniel and Whitteridge, '61; Van Essen et al., '84). This allowed a direct comparison of cortical and LGN topographies in the same hemisphere. Complete results from two such experiments are shown in Figure 11. Above the LGN laminar maps are maps of the corresponding striate cortex showing the location of injection sites. In Figure 11A, a cortical injection had been made along the horizontal meridian representation at an eccentricity of about 6–8°. The label in each LGN layer was in approximately the location expected from the topographical maps presented above. In layers 2 and 3, the label is somewhat closer to the upper margin, suggesting a biased representation of inferior fields in a different set of layers than was found in the Malpeli and Baker case (cf. Fig. 8).

In Figure 11B, three injections of ^{3}[H]-proline had been made in striate cortex, with two (sites 1 and 2) including the horizontal meridian representation, and one (site 3) in the inferior field representation at roughly the same eccen-

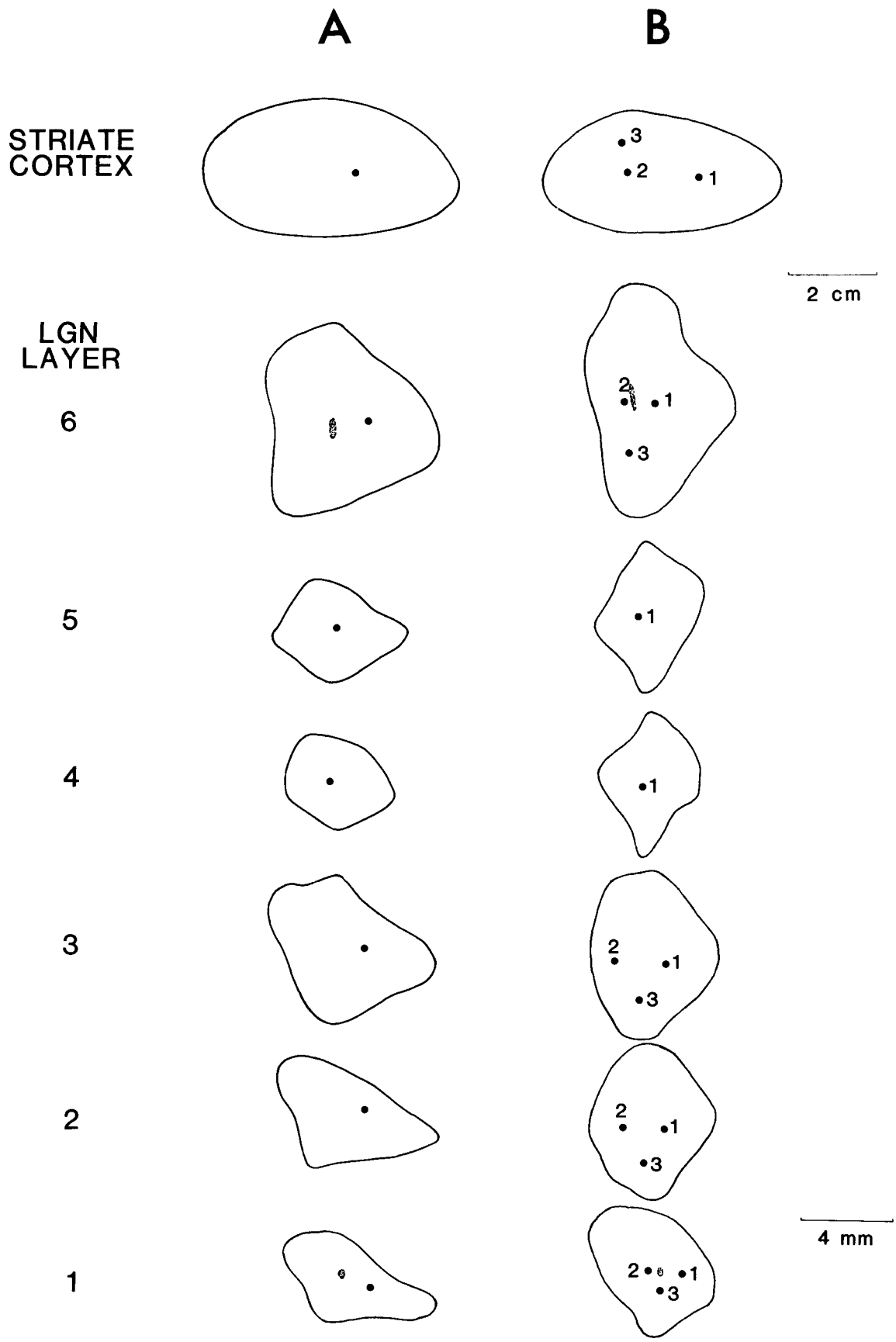
A
B
STRIATE CORTEX
LGN LAYER
6
5
4
3
2
1
2 cm
4 mm

tricity as site 2. Label from these injections was present in each principal layer, and, as expected, the labeling sites in the LGN maps were topologically inverted with respect to injection sites in cortex (see "Discussion"). In striate cortex, the separation between sites 1 and 2 is significantly larger than that between sites 2 and 3. Interestingly, in LGN layer 6, the opposite is true. Since it is known that the cortical representation is approximately isotropic along the horizontal meridian (Van Essen et al., '84), this provides an anatomical confirmation that the LGN layer 6 representation is strongly anisotropic in the same region. The configuration of labeled patches in other layers suggests that the anisotropy was present, but smaller, in layers 2 and 3, and that it was absent altogether in layer 1.

The location of the optic disc representation in layers 1 and 6 was quite variable. In layer 6, it ranged from less than one-half to more than three-quarters of the way from the dorsal to the ventral pole, while in layer 1, it varied from one-half to two-thirds of the corresponding distance. Given that the optic disc is in a relatively fixed position within the retina, this indicates that there is significant individual variability in geniculate topography, an interpretation that is consistent with the variability in tracer labeling and laminar shapes described above. In the macaque retina, the optic disc is somewhat elongated orthogonally to the horizontal meridian (about 1.3–1.4 times as long as wide; Polyak, '57; Malpeli and Baker, '75). Its representation in layer 6, though, was considerably more elongated in the three cases in which it was carefully mapped (Fig. 10). Again, this is consistent with an anisotropic representation of the visual field in layer 6 near the horizontal meridian, favoring directions along lines of isoeccentricity. The layer-1 representation of the optic disc was difficult to determine precisely, but it appeared to be about circular or slightly elongated roughly parallel to the presumed direction of the horizontal meridian representation (see Fig. 5).

DISCUSSION

The principal contribution of this study has been to provide maps of visual topography in each layer of the LGN. Our evidence indicates that the magnocellular and parvicellular divisions of the LGN differ in several respects and that the representation of the visual field is anisotropic over a large part of the LGN. In addition, we obtained quantitative estimates of the number of LGN cells as a function of eccentricity for each layer. There appear to be significant individual differences in some of the quantitative aspects of LGN organization, but the major qualitative features (anisotropies and differential emphasis on central vision) were confirmed in additional cases besides the one examined in greatest detail.

Fig. 11. A comparison of LGN and cortical topography in two monkeys. In each case, injections of [^{3}H]-proline were made in striate cortex, at locations indicated by the dots on the two-dimensional maps of striate cortex (in their standard configuration, with the foveal representation to the right and the far periphery to the left). The centers of labeled regions in the LGN layers are indicated by dots. The optic disc representations are outlined by broken lines in layers 1 and 6.

Malpeli and Baker ('75) calculated magnification factors for the LGN based on the LGN volumes representing different eccentricity ranges (their Table 1 and Figure 13). When their data are fitted to a power function with eccentricity, magnification is found to be proportional to $E^{-1.64}$. However, Malpeli and Baker did not account for changes in cell density in their estimates of magnification factor. When the function relating magnification to eccentricity is adjusted for this, cellular representation is proportional to $E^{-1.80}$, in reasonable agreement with our own finding that the overall representation is proportional to $E^{-1.90}$. It was not apparent from their study, however, that there are significant differences in the slope of this power function, and thus on the emphasis on central vision, for parvicellular vs. magnocellular layers.

The parvicellular and magnocellular representations of visual space

The parvicellular and magnocellular divisions differ significantly in their representations of the visual field, both in their cellular magnification as a function of eccentricity and in their anisotropies. These differences can be related in an interesting way to the three-dimensional architecture of the LGN. Figure 12 is a posterior view of layers 1 and 6 of the LGN model, shown in their proper three-dimensional configuration but in the absence of the remaining layers. A series of visual field compartments forming a hemi-annulus of constant eccentricity is shown to the left. The representations of these compartments have been drawn on layers 1 and 6, and the connections between corresponding compartments in the two layers show the lines of projection running between layers. Since layer 1 is the innermost of the laminar half-cylinders, its mediolateral circumference is smallest; corresponding to this, the layer-1 compartments are compressed along lines of isoeccentricity (which run approximately mediolaterally) relative to those of the other geniculate layers. On the other hand, layer 6, the outermost layer, has compartments that are longest along lines of isoeccentricity. The length ratio of isoeccentricity segments to isopolar segments for each compartment is largest in layer 6 and smallest in layer 1; the intervening layers have intermediate values of this ratio. As a consequence, the anisotropies of the magnocellular layers are different from those of the parvicellular layers. The pronounced anisotropy along the peripheral horizontal meridian representation in layers 3 and 6 cannot be entirely accounted for by these simple geometrical considerations, however. These anisotropies may also be correlated with the biased distribution of ganglion cells along the horizontal meridian in the macaque retina (Stone and Johnston, '81).

In terms of laminar surface area, the relative emphasis on central vision is only slightly larger in the parvicellular principal layers than in the magnocellular (Fig. 8). As mentioned previously, the difference between parvicellular and magnocellular layers is enhanced by several factors, including the presence of parvicellular leaflets representing only central vision and the occurrence of gradients in cell density and laminar thickness of parvicellular layers. In terms of cell numbers, our calculations indicate that there are about four parvicellular cells for every magnocellular cell in the far periphery (80° eccentricity), whereas in the foveal representation (1°) this ratio is closer to 40.

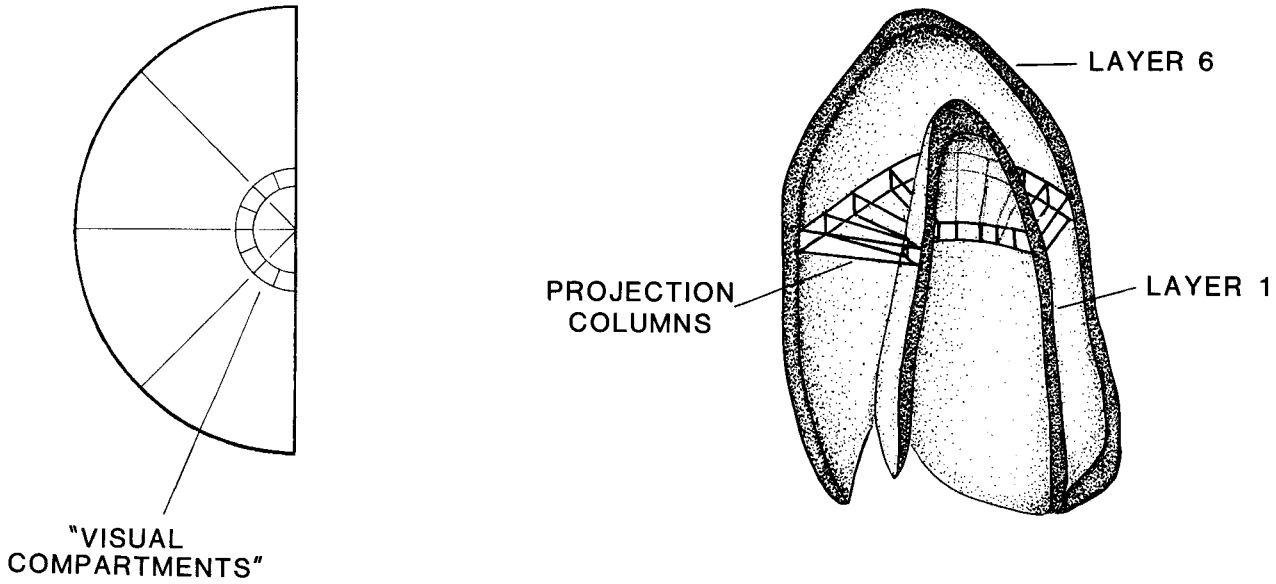

Fig. 12. A. The visual field, with several square compartments of equal eccentricity included. B. Layers 1 and 6 of the LGN, after removal of the other four layers, viewed from a posterior aspect. The regions of layers 1 and 6 corresponding to the compartments of Figure 14A are shown, as are lines of projection between corresponding points in the two layers. The cylindrical geometry of the LGN ensures that the layer-6 representations of visual field compartments are elongated mediolaterally relative to those in layer 1.

Ipsilateral vs contralateral eye representation

In both the magnocellular and parvicellular segments of the LGN, the total number of cells receiving inputs from the contralateral eye is larger than that from the ipsilateral eye. Not surprisingly, the contralateral bias in the parvicellular layers is most pronounced in the representation of the visual periphery (including the monocular crescent). The greater contralateral eye representation in the parvicellular layers is also consistent with the concentric array of laminae in the LGN: The contralateral eye projects to layers 4 and 6, which surround, and are therefore larger than, layers 3 and 5. For the magnocellular laminae, layer 2 (ipsilateral input) is slightly larger than layer 1 (contralateral input), but layer 1 is typically somewhat thicker than layer 2. Clark ('41) estimated that, in the magnocellular LGN, 60% of all cells are contralaterally innervated. Our estimate of 54%, taking into account the thicknesses and areas of layers 1 and 2, is in reasonable agreement with this.

Recently, complete two-dimensional reconstructions of striate cortex and its ocular dominance stripes in layer 4C have been prepared (Connolly et al., '82; LeVay et al., '84). In the region where the visual periphery is represented on the maps, the area of ipsilateral eye stripes is significantly less than that of the contralateral eye stripes. Moreover, this bias is strongest along the horizontal meridian. These findings suggest that the contralateral eye bias in the LGN is retained in the projection to striate cortex.

Individual variability in the LGN

Striate cortex and the layers of the LGN show individual variability in their size, shape, and topography, but in different ways. For instance, while the area of layer 6 varied only moderately (40–55 mm^2) in the eight cases from the present study, two-dimensional maps of striate cortex span a more than twofold range in surface area (695–1,560 mm^2; Van Essen et al., '84). On the other hand, the shape of unfolded LGN layers is apparently more variable than that of striate cortex, which is approximately elliptical in all maps that have been prepared. The extensive rotations, torques, and transverse compression that the LGN is subject to during its development and in the course of its migration through the brain during enlargement of the thalamus (Rakic, '77) may contribute substantially to the individual variability in its adult shape and in the shape of its unfolded layers. There is significant individual variability in visual topography of striate cortex (Van Essen et al., '84), and evidence has been presented in the present study that this is also true for the LGN.

A topological inversion in the geniculocortical projection

In the course of comparing the visual field representations in the LGN and striate cortex, we became aware of a complexity in their relationship that has not to our knowledge been described previously. The nature of this relationship is illustrated in Figure 13, which shows schematic

views of the LGN and striate cortex in three progressively more abstract configurations. Figure 13A shows a medial view of the right hemisphere of a macaque brain with the LGN shaded in and the margin of striate cortex indicated by a dotted line. In Figure 13B, the LGN and striate cortex are shown isolated, but still in their natural relationship to one another. In order to illustrate the topology of this relationship, four selected geniculocortical fibers, respectively representing foveal (F), peripheral (P), inferior (I), and superior (S) parts of the visual field, have been drawn in from their exit at the dorsal surface of the LGN to their entry into striate cortex. In Figure 13C, striate cortex and LGN layer 6 have been schematically unfolded and rotated to their standard orientation for two-dimensional maps without disconnecting any of the geniculocortical fibers. It is evident that in this configuration there is a crossing-over of fibers along the superior-inferior axis but not along the foveal-peripheral axis. It is possible to change the axis along which inversion occurs by rotating one surface relative to the other, but it is not possible to eliminate the

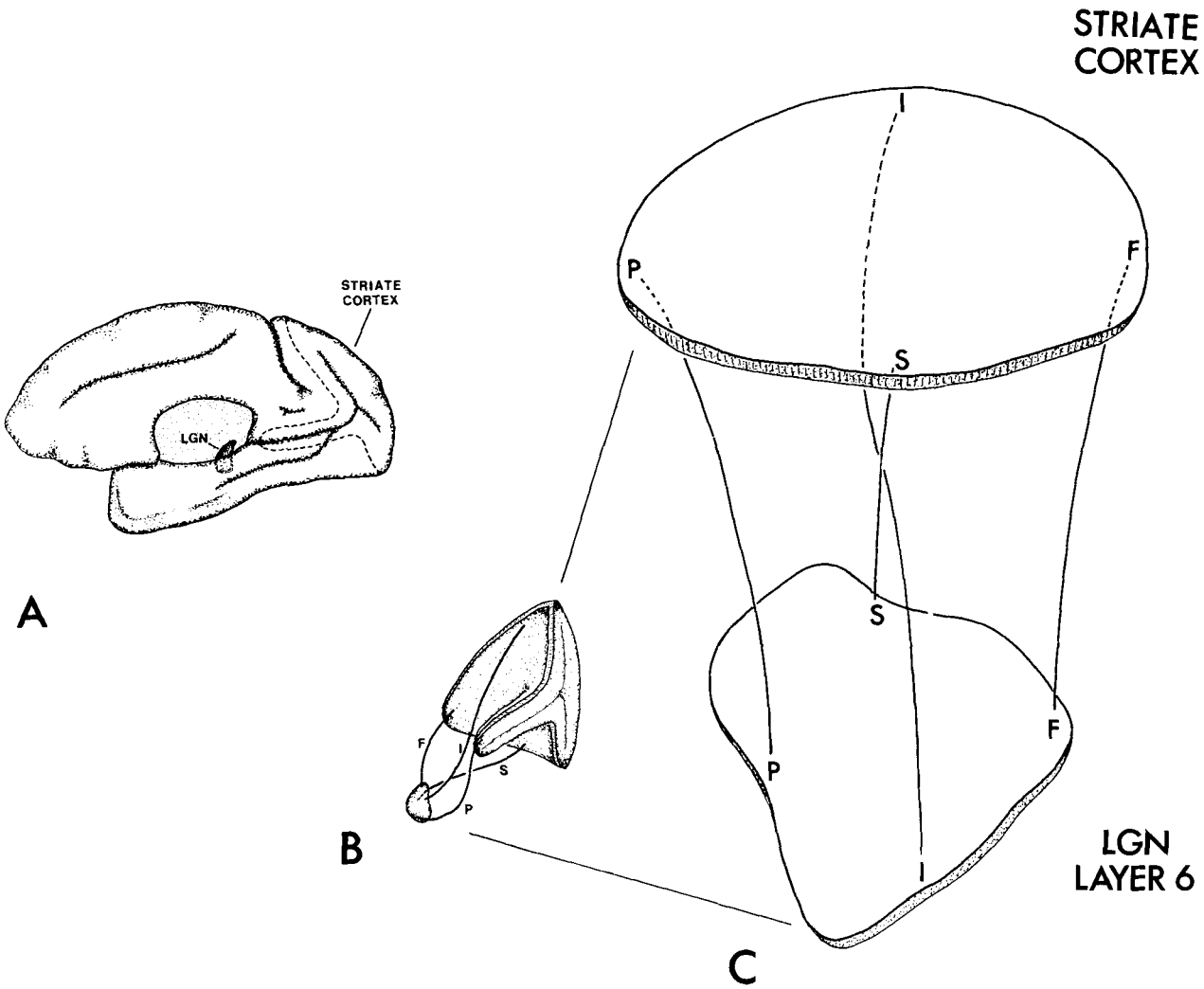

Fig. 13. The topography of striate cortex is topologically inverted with respect to that of the LGN. A. The LGN and the medial wall of cerebral cortex, with the borders of striate cortex indicated by the dashed line. B. LGN and striate cortex from a medio-anterior perspective, with schematic optic radiation fibers from the convex surface of the LGN to striate cortex connecting equivalent regions of the visual representations. F, fovea; P, far periphery; I, inferior vertical meridian; S, superior vertical meridian. C. The unfolded maps of striate cortex and LGN layer 6, connected by the same radiation fibers. Inversion about an axis is required to make the two representations overlay. This relationship between cortical and LGN topographies can be easily confirmed by making carboard cutouts of LGN and cortical maps and connecting them in appropriate fashion by pieces of string.

inversion altogether without flipping one of the maps completely (or, equivalently, by having the axons leave the LGN or enter the cortex from the opposite side). The significance of this topological complexity is most apparent in relation to the issue of how an orderly geniculocortical projection is established during development. In a general sense, one way to establish an orderly mapping from one structure to another is for all fibers to preserve their neighborhood relationships as they grow to their target. However, if it is necessary that there be a systematic crossing-over of fibers along one axis, then it is difficult to envision that a topographic map in the target structure could be established exclusively by local fiber-fiber interactions.

It is unclear whether there is any advantage associated with topological inversions in the geniculocortical pathway, but its occurrence is not unique to the macaque. Based on the available evidence on the topographic organization of the LGN and striate cortex and on the side from which geniculocortical fibers exit the LGN, a similar relationship can also be inferred for other primates (Kaas et al., '72; Allman and Kaas, '71) and for the cat (Sanderson, '71; Tusa et al., '78). The inversion can even be inferred from what is known of the human geniculostriate pathway (Polyak, '57) even though it is not obvious just from looking at Polyak's drawings of the course of the optic radiation in humans (his Figs. 235, 236). Thus, a topological reordering may be a consistent feature of mammalian geniculostriate projections.

This raises the broader question of how common such topological inversions are for other topographically ordered sensory projections. For example, V2 is an area which in all species examined shares a vertical meridian representation with V1 (striate cortex) and is organized in mirror-image fashion (Van Essen, '79). From this it can be inferred that V1 projects to V2 in noninverted fashion and that the same must be true for the projection from the LGN to V2 in species (such as the cat) where this projection exists. Likewise, in primates the topographic organization of MT (Allman and Kaas, '71; Van Essen et al., '81) is such that the projection to it from V1 is noninverted and from V2 is inverted. In general, it appears that both inverted and noninverted projections are common in the central nervous system. Indeed, it would be difficult to avoid this in any system having a large number of pathways interconnecting a collection of topographically organized, laminated structures. Thus, it is likely that developmental strategies capable of handling both types of mapping must have arisen early in mammalian evolution, if not before.

This conclusion is of interest in relation to what is known about retinal projections and the organization of the optic nerve. In some vertebrate species, there is a high degree of topographic ordering within the optic nerve, but the order does not preserve all neighborhood relationships within the retina and thus is topologically not equivalent to the retinal surface. Moreover, there is considerable topological reorganization that occurs along the course of the optic nerve and optic tract (Scholes, '79; Easter et al., '81). These complexities may be related to either of two special features of the retina: It is distinctive from a developmental standpoint, being a structure that grows by circumferential addition of cells, and it is also distinctive topologically, being an annular structure with a central hole through which retinal ganglion cell axons are funneled to form the optic nerve. In any event, the present analysis emphasizes that a variety of developmental strategies are likely to be used in the formation of orderly maps within the central nervous system.

Relationship of retinal, geniculate, and cortical representations

One instructive way of analyzing the transformation in the geniculocortical pathway, shown in Figure 14, is to view the map of layer 6 LGN topography (Fig. 14B) alongside that of striate cortex (Fig. 14C), as determined previously (Van Essen et al., '84). The central 5° of the visual field is stippled on both maps as well as in the visual field to illustrate the greater emphasis on central vision in striate cortex, where 42% of the map is devoted to the central 5°, compared to that in LGN layer 6, where the corresponding value is only 20%.

Another interesting pattern evident in this Figure is the consistent difference in the anisotropies of the geniculate and cortical representations. The anisotropies in representative regions can be readily assessed by noting the shapes of the various darkened compartments in each map. Along the horizontal meridian the representation is nearly isotropic in striate cortex, but in LGN layer 6 there is a roughly twofold anisotropy in favor of directions along lines of isoeccentricity ($M_p/M_e \approx 2$). More generally, the index of anisotropy, if defined as the ratio of isopolar to isoeccentricity magnification (M_p/M_e), is approximately twice as great in striate cortex as in LGN layer 6 over most of the visual representation. A similar relationship holds, though less consistently, for the comparison between striate cortex and LGN layer 5, while for layers 1 through 4 the geniculate anisotropies are not consistently different than those for striate cortex. Related to this is the fact that the shapes of the deeper LGN layers (1–3) are elongated much like that of striate cortex, whereas the shape of layer 6 is much closer to circular.

A scheme that may help to clarify how the cortex can have anisotropies that differ substantially from those of the LGN layers providing a large fraction of its input is shown in Figure 15. The representation of three small compartments of the visual field near the horizontal meridian is shown to the right (Fig. 15A) for LGN layers 6 and 5. Suppose that the anisotropy initially present in these layers is preserved as they project to cortical layer 4C and that the strips for each eye are aligned side by side rather than end to end (i.e., joined along their isoeccentricity contours, not their isopolar contours). The justification for this kind of juxtaposition is that ocular dominance stripes tend to run parallel to isoeccentricity contours over much of striate cortex (LeVay et al., '75, '84; Hubel and Freeman, '77; Connolly et al., '82). This arrangement would lead to a representation outside cortical layer 4C that was isotropic, as is actually found in this part of striate cortex. Along the vertical meridian, where the LGN layer 6 and 5 inputs are isotropic, the same rule of juxtaposition would produce a cortical anisotropy of the orientation actually observed.

This hypothesis has the attractiveness of accounting for the substantial differences in cortical and geniculate an-

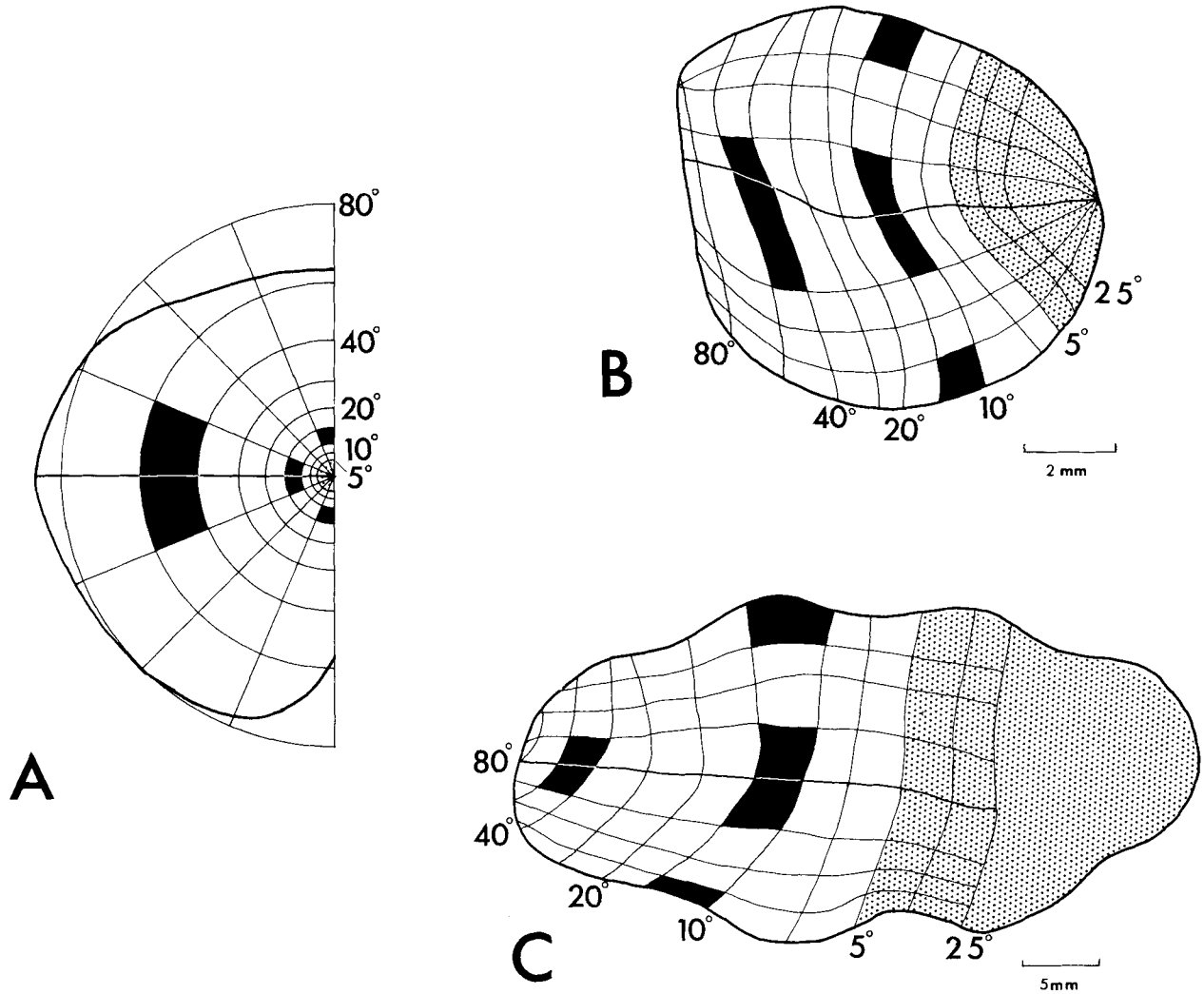

Fig. 14. The visual field (A) and its representations in LGN layer 6 (B) and striate cortex (C) (Van Essen et al., '84). As in Figure 8, the visual field has been divided into small, approximately square regions by a grid of isoeccentricity and isopolar angle lines. The transformations of this grid are shown on the layer-6 and cortical maps. The darkened line in Figure 16A represents the perimeter of the macaque visual field. (Note inverted cortical and LGN maps.) The central 5° of the visual representation has been stippled in A, B, and C. Several visual field compartments along the horizontal or vertical meridia and their corresponding LGN and cortical representations have been darkened for comparison.

isotropies in terms of a simple rule for combining inputs from two eyes into what is ultimately a single binocular map in visual cortex. It could also account for the observation of Hubel et al. ('74) that the representation in layer 4C is anisotropic, if one assumes that their recordings were somewhere near the horizontal meridian representation. On the other hand, it is unclear how this scheme should be expanded to include the integration of inputs from the remaining LGN layers, where the anisotropies are not the same as in layers 6 and 5.

Another useful way of examining the relationship between visual centers is to compare the relative numbers of cells devoted to any given part of the visual field. For the geniculocortical pathway, we used the expressions for cellular magnification for each LGN layer obtained in the present study and the expression for areal magnification in striate cortex obtained previously (Van Essen et al., '84), adjusted by the cell counts for different layers determined by O'Kusky and Colonnier ('82). Figure 16 shows three different cellular ratios plotted as a function of eccentricity: 1) total number of striate neurons per LGN neuron; 2) number of layer 4A and 4Cβ neurons (i.e., those in parvicellular-recipient layers) per parvicellular neuron; and 3) number of layer 4Cα neurons per magnocellular neuron.

Various sources of inaccuracy in our quantitative analysis of LGN topography have been discussed in preceding sections, and it is appropriate to consider their implications for interpreting the curves in Figure 16. The uncertainties are neither so small as to be completely negligible, nor so large as to render the curves meaningless. Unfortunately, it is not possible to calculate precise uncertainty limits, given the diverse nature of the different sources of error and the difficulty in assessing their exact magnitude. Our best estimate, once all sources of error are taken into consideration, is that the points on each of the curves have an absolute accuracy of a factor of two or three, and that the

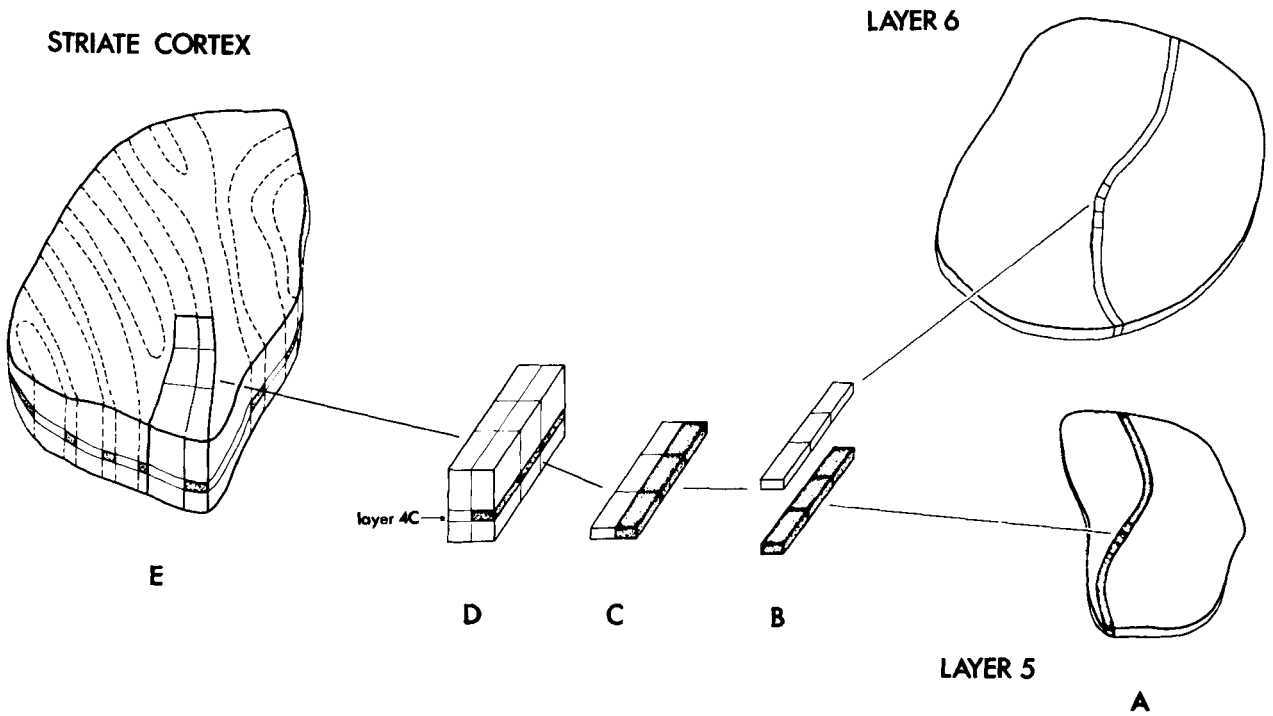

Fig. 15. On the right, the anisotropic layer-5 and layer-6 representations of small squares in the visual field near the horizontal meridian (A). These representations send anisotropic inputs (B) to striate cortex, which, when they converge on layer 4C (C), produce an isotropic visual representation in cortical "modules" (D). In E, the cortical modules are shown inserted into a slice of striate cortex.

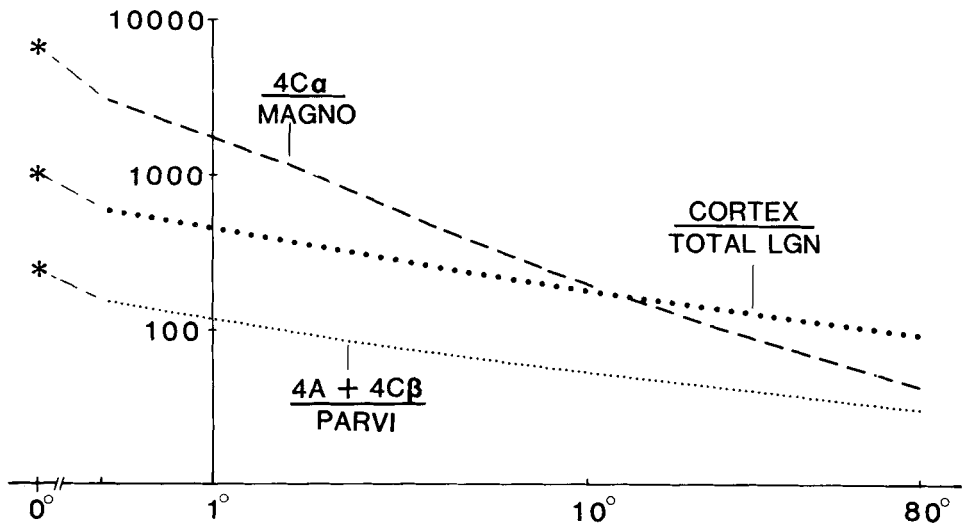

Fig. 16. Cell ratios as a function of eccentricity in the geniculocortical pathway. The large-dot line shows the total number of striate nerons per LGN cell. This ratio was calculated as M_a (cortex) × (cells/mm^2 surface area)/M_c (LGN), where M_a (cortex) is the areal magnification factor for a standardized striate cortex (equation 8 from Van Essen et al., '84); cells/mm^2 was taken from O'Kusky and Colonnier ('82), and M_c (LGN) is the total LGN cellular magnification factor from Table 1. The small-dot line shows the number of 4A and 4Cβ cells per parvicellular cell, calculated as M_a (cortex) × (4A + 4Cβ cells/mm^2) × M_c (parvi), with appropriate data from the same three sources. The dashed line shows the number of 4Cα cells per magnocellular cell, calculated as M_a (cortex) × (4Cα cells/mm^2) × M_c (magno).

relative accuracy (comparing different points on the same curve) is significantly better than this. With these provisos in mind, there are several noteworthy observations to be made.

All of the curves in Figure 16 have a significant downward slope.This supports the suggestion by Malpeli and Baker ('75) that the distribution of geniculocortical fibers to striate cortex is uneven, with a lower density of LGN projections to the fovea than to the periphery. The ratio of 4A and 4Cβ to parvicellular neurons extends over about an eightfold range, from 240 at 0° eccentricity to 30 in the far periphery. The ratio of 4Cα to magnocellular cells spans more than a 150-fold range, from about 7,000 at 0° to 45 in the periphery. In view of this, it would be of interest to know whether the size of geniculocortical terminations in layers 4Cα and 4Cβ varies with eccentricity. Blasdel and Lund ('83) have found that the extent of different fiber arborizations is about sixfold greater in 4Cα than in 4Cβ in the (unspecified) region of cortex that they studied. This is in reasonable agreement with the eightfold difference in cell number in parvicellular vs. magnocellular layers (Clark, '41), but a wider range will need to be explored to ascertain whether arbor sizes depend significantly on eccentricity.

Precise quantitative relationships between the retina and the geniculate are more difficult to assess because of the displacement of retinal ganglion cells in the foveal region. Nonetheless, it is evident from the data of Rolls and Cowey ('70) that retinal ganglion cell density is only about 50 times greater at 1° than at 80° eccentricity. This contrasts with a ratio of 870 for the cellular magnification at 1° vs. 80° in the LGN. Thus, despite the fact that the estimated total number of LGN cells (1.3×10^6, present study; 1.6×10^6, Clark, '41; 1.1×10^6, Chow et al., '50) is similar to the total number of retinal ganglion cells (1.1×10^6, Rolls and Cowey, '70), their ratio must vary from many LGN cells per retinal ganglion cell for the fovea to fewer than one LGN cell per retinal ganglion cell in the periphery, as was originally pointed out by Malpeli and Baker ('75). In order to delineate this relationship more exactly, it will be necessary to obtain separate counts of the distribution of retinal ganglion cells projecting to parvicellular and magnocellular layers. This task is likely to be aided by the distinctive morphology of these two cell types (Perry and Cowey, '81; Leventhal et al., '81).

ACKNOWLEDGMENTS

This work was supported by NIH Grant R01 EY 02091. We thank C. Shotwell for histological work and preparation of figures, C. Oto and C. Hochenedel for typing the manuscript, and J.H.R. Maunsell for comments on the manuscript.

LITERATURE CITED

Allman, J., and J.H. Kaas (1971) Representation of the visual field in striate and adjoining cortex of the owl monkey (*Aotus trivirgatus*). Brain Res. *35*:89–106.

Blasdel, G.G., and J.S. Lund (1983) Afferent axons in layer 4c of macaque striate cortex. J. Neurosci. *3*:1389–1413.

Chow, K.-L., J.S. Blum, and R.A. Blum (1950) Cell ratios in the thalamocortcortical visual system of Macaca mulatta. J. Comp. Neurol. *92*:227–239.

Clark, W.E. Le Gros (1941) The laminar organization and cell content of the lateral geniculate body in the monkey. J. Anat. *75*:419–433.

Connolly, M., S. Le Vay, and D.C. Van Essen (1982) The complete pattern of ocular dominance stripes in macaque striate cortex. Soc. Neurosci. Abstr. *8*:676.

Daniel, P.M., and D. Whitteridge (1961) The representation of the visual field on the cerebral cortex in monkeys. J. Physiol. (Lond.) 159:203–221.

Dreher, B., Y. Fukada, and R.W. Rodieck (1976) Identification, classification and anatomical segregation of cells with X-like and Y-like properties in the lateral geniculate nucleus of old-world primates. J. Physiol. (Lond.) *258*:433–452.

Easter, S.S., A.C. Rusoff, and P.E. Kish (1981) The growth and organization of the optic nerve and tract in juvenile and adult goldfish. J. Neurosci. *1*:793–811.

Hassler, R. (1966) Comparative anatomy of the central visual systems in day-and-night-active primates. In R. Hassler and H. Stephan (eds): Evolution of the Forebrain. Stuttgart: Thieme, pp. 519–534.

Hubel, D.H., and D.C. Freeman (1977) Projection into the visual field of ocular dominance columns in macaque monkey. Brain Res. *122*:336–343.

Hubel, D.H., and T.N. Wiesel (1972) Laminar and columnar distribution of geniculocortical fibers in the macaque monkey. J. Comp. Neurol. *146*:421–450.

Hubel, D.H., T.N. Wiesel, and S. Le Vay (1974) Visual field representation in layer IVc of monkey striate cortex. 4th Ann. Meet. Soc. Neurosci. Abstr., p. 264.

Kaas, J.H., R.W. Guillery, and J.M. Allman (1972) Some principles of organization in the dorsal lateral geniculate nucleus. Brain Behav. Evol. *6*:253–299.

Kass, J.H., M.F. Huerta, J.T. Weber, and J.K. Harting (1978) Patterns of retinal terminations and laminar organizations of the lateral geniculate nucleus of primates. J. Comp. Neurol. *182*:517–541.

Kaplan, E., and R.M. Shapley (1982) X and Y cells in the lateral geniculate nucleus of macaque monkeys. J. Physiol. (Lond.) *350*:125–143.

LeVay, S., M. Connolly, J. Houde, and D.C. Van Essen (1984) The complete pattern of ocular dominance stripes in the striate cortex and visual field of the macaque monkey. J. Neurosci. (submitted).

Le Vay, S., D.H. Hubel, and T.N. Wiesel (1975) The pattern of ocular dominance columns in macaque visual cortex revealed by a reduced silver stain. J. Comp. Neurol. *159*:559–576.

Leventhal, A., R.W. Rodieck, and B. Dreher (1981) Retinal ganglion cell classes in the old world monkeys: Morphology and central projections. Science *213*:1139–1142.

Lund, J.S., R.D. Lund, A.E. Hendrickson, A.H. Bunt, and A.F. Fuchs (1976) The origin of efferent pathways from the primary visual cortex, area 17, of the macaque monkey as shown by retrograde transport of horseradish peroxidase. J. Comp. Neurol. *164*:287–304.

Malpeli, J.G., and F.H. Baker (1975) The representation of the visual field in the lateral geniculate nucleus of Macaca mulatta. J. Comp. Neurol. *161*:569–594.

O'Kusky, J., and M. Colonnier (1982) A laminar analysis of the number of neurons, glia and synapses in the visual cortex (area 17) of adult macaque monkeys. J. Comp. Neurol. *210*:278–290.

Perry, V.H., and A. Cowey (1981) The morphological correlates of X- and Y-like retinal ganglion cells in the retina of monkeys. Exp. Brain Res. *43*:226–228.

Polyak, S. (1957) The Vertebrate Visual System. Chicago: University of Chicago Press.

Rakic, P. (1977) Genesis of the dorsal lateral geniculate nucleus in the rhesus monkey: Site and time of origin, kinetics of proliferation, routes of migration and pattern of distribution of neurons. J. Comp. Neurol. *176*:23–52.

Rolls, E.T., and A. Cowey (1970) Topography of the retina and striate cortex and its relationship to visual acuity in rhesus monkeys and squirrel monkeys. Exp. Brain Res. *10*:298–310.

Sanderson, K.J. (1971) The projection of the visual field to the lateral geniculate and medial interlaminar nuclei in the cat. J. Comp. Neurol. *143*:101–118.

Schiller, P.H., and J.G. Malpeli (1978) Functional specificity of lateral geniculate nucleus laminae of the rhesus monkey. J. Neurophysiol. *41*:788–797.

Scholes, J.H. (1979) Nerve fibre topography in the retinal projection to the tectum. Nature *278*:620–624.

Stone, J., and E. Johnston (1981) The topography of primate retina: A study of the human, bushbaby and new- and old-world monkeys. J. Comp. Neurol. *196*:205–223.

Tusa, R.J., L.A. Palmer, and A.C. Rosenquist (1978) The retinotopic organization of Area 17 (striate cortex) in the cat. J. Comp. Neurol. *177*:213–236.

Van Buren, J.M. (1963) The Retinal Ganglion Cell Layer. Springfield, IL: Thomas.

Van Essen, D.C. (1979) Visual areas of the mammalian cerebral cortex. Ann. Rev. Neurosci. *2*:227–263.

Van Essen, D.C., and J.H.R. Maunsell (1980) Two-dimensional maps of the

cerebral cortex. J. Comp. Neurol. *191:*255–281.

Van Essen, D.C., J.H.R. Maunsell, and J.L. Bixby (1981) The middle temporal visual area in the macaque: Myeloarchitecture, connections, functional properties and topographic organization. J. Comp. Neurol. *199:*293–326.

Van Essen, D.C., W.T. Newsome, and J.H.R. Maunsell (1984) The visual field representation in striate cortex of the macaque monkey: Asymmetries, anisotropies, and individual variability. Vision Res. *24:*429–448.